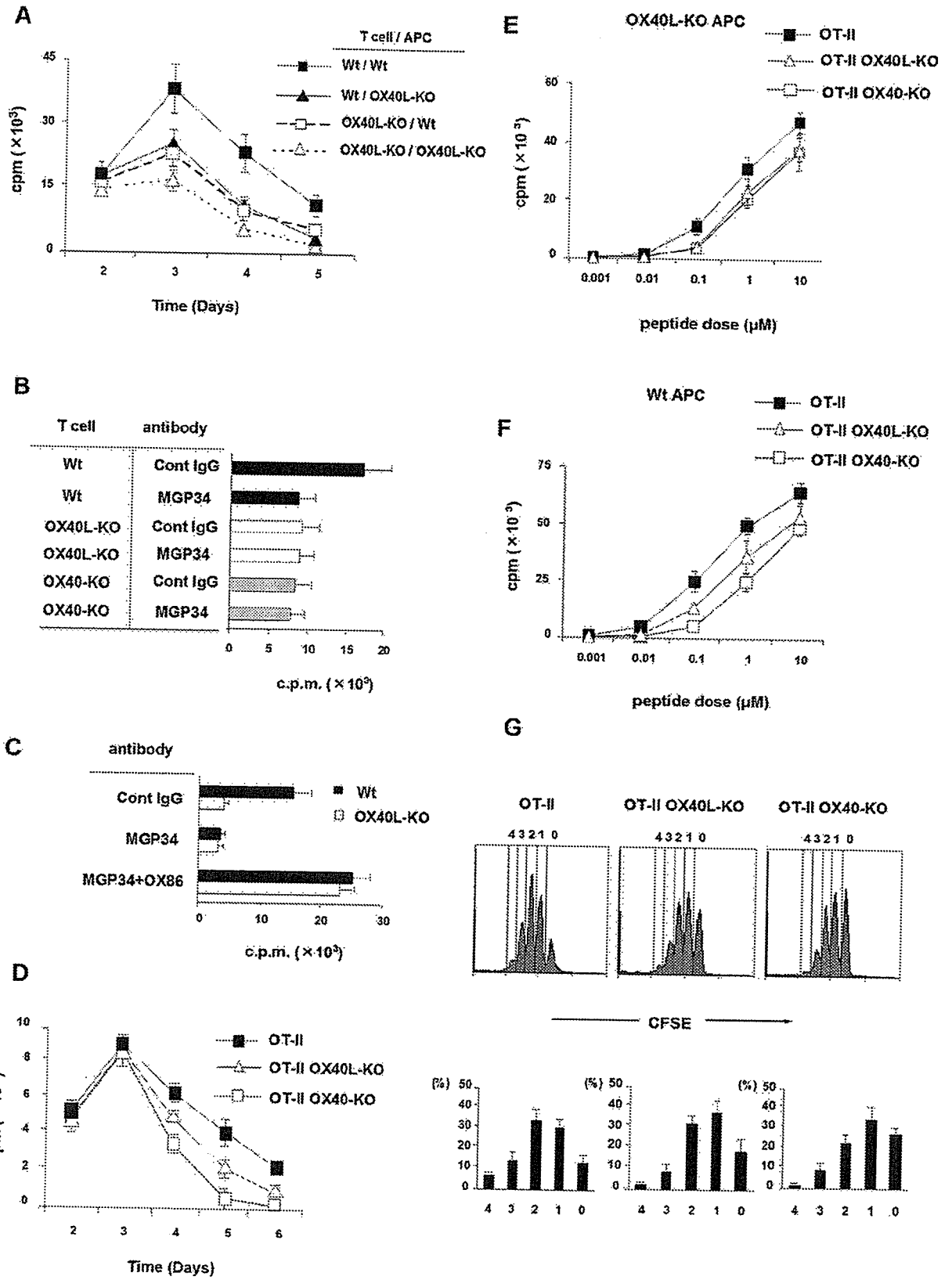

FIGURE 4. OX40L expression on T cells is required for the optimal proliferation of Ag-specific T cells. *A*, Purified $CD4^+$ T cells (5×10^4) from wild-type or OX40L-KO mice were stimulated with soluble anti-CD3 mAb (10 μg/ml) in the presence of irradiated wild-type or OX40L-KO splenocytes (APCs) (2×10^5). At the indicated days, [^{3}H]thymidine incorporation during the last 8 h of cultures was measured as an indicator of cell proliferation and is expressed as the mean (±SD) of triplicate cultures. Similar results were obtained in at least three independent experiments. *B* and *C*, Purified $CD4^+$ T cells (1×10^5) from wild-type (■), OX40L-KO (□), and OX40-KO (▨) mice were stimulated with plate-bound anti-CD3 mAb (5 μg/ml) in the absence of APCs. An inhibitory anti-OX40L mAb (MGP34; 20 μg/ml), control rat IgG (cont IgG; 20 μg/ml), or anti-OX40L mAb, plus an agonistic anti-OX40 mAb (MGP34 and OX86; 10 μg/ml each) were added, as indicated. [^{3}H]Thymidine incorporation during the last 8 h (*Figure legend continues*)

conclusion that OX40L on T cells, as well as OX40L on APCs, can provide potent costimulatory signals to regulate the proliferative response of CD4 T cells.

Optimal T cell survival is dependent on the OX40L expression on T cells after Ag priming

The reduction in late T cell proliferation seen in OX40L-deficient T cells (Fig. 4*D*) may reflect impaired T cell survival due to decreased OX40 signals. To address whether long-term T cell survival is directly controlled by OX40L on T cells, OT-II, OT-II OX40-KO, and OT-II OX40L-KO T cells were stimulated by OVA-loaded OX40L-deficient or OX40L-sufficient wild-type APCs, and the cells' viability was monitored. OT-II OX40L-KO and OT-II OX40-KO T cells stimulated in the presence of OX40L-deficient APCs, which could not provide any OX40 signals, showed a marked reduction in survival during the 15 days of Ag stimulation (Fig. 5*A*). In the presence of OX40L-expressing APCs, OT-II OX40L-KO T cells, which are capable of receiving the OX40 signal only through APCs, showed a 85% reduction in their ability to survive compared with OT-II T cells 15 days after Ag stimulation (Fig. 5*B*, *right panel*). Similarly to the proliferation assay, survival analysis reveals that OX40L on T cell has a great impact on accumulation of T cells during the contraction phase. Furthermore, adding an inhibitory anti-OX40L mAb, which can bind to OX40L on T cells only when OX40L-KO APCs are used, dramatically suppressed the T cell survival during the 15 days of culture (Fig. 5*C*). Similarly, the suppressive effect of the OX40L-blocking mAb was rescued by cross-linking the OX40 receptor on T cells when agonistic anti-OX40 mAb was added (Fig. 5*C*). The reduction in T cell survival due to the absence of functional OX40L on T cells raises the question of whether the OX40-OX40L interaction on T cells imprints the cells for survival during early Ag priming or directly promotes cell survival during the late effector phase. To address this question, OT-II T cells were stimulated by OVA-loaded OX40L-deficient or OX40L-sufficient APCs, and T cell survival was analyzed 10 days poststimulation. To block the OX40-OX40L interaction, the anti-OX40L mAb was added for the initial 3 days, the last 7 days, or for all 10 days. As shown in Fig. 5*D*, blocking the OX40-OX40L interaction on T cells during either the early or later phase significantly diminished the survival of the CD4 T cells, while adding it for the entire 10 days had the most suppressive effect on T cell survival. Thus, OX40-OX40L interactions on T cells during both early and later phases of Ag priming contribute to the long-term survival of Ag-specific CD4 T cells. Collectively, these findings emphasize the functional importance of the OX40-OX40L interaction during T cell-T cell contact, in that this interaction supports long-term CD4 T cell survival.

OX40L expression on T cells promotes long-term survival of CD4 T cells in vivo

To evaluate the in vivo role of OX40L expression on T cells, we first examined the expression of OX40L on activated OT-II T cells in vivo. To achieve this, Ly-5.2$^+$ OT-II cells were transferred into wild-type non-OT-II recipient mice (Ly-5.1$^+$), followed by immunization of the recipient mice with OVA/LPS. One and 2 days postimmunization, donor T cells were sorted magnetically from the spleen and lymph nodes of the recipient mice, and the expression level of the *OX40L* transcript in the donor T cells was determined by real-time PCR. Although the *OX40L* transcript was not detected in naive OT-II T cells, a significant induction of OX40L was observed following the OVA immunization (Fig. 6*A*). Although the induction of *OX40L* mRNA was readily detectable, we did not detect any surface expression of OX40L on the activated donor T cells by flow cytometry. We suspect that, as in our in vitro experiments (Fig. 2), the absence of OX40L on the surface of donor T cells may be due to the presence of OX40 expression on donor T cells and the adjacent cells of the recipient mice. To address this, Ly-5.1$^+$ OT-II and OT-II OX40-KO CD4 T cells were transferred into congenic Ly-5.2$^+$ wild-type and OX40-KO recipient mice, followed by Ag immunization. Three days after immunization, in contrast to negligible OX40L expression on OT-II cells that had been transferred to wild-type recipient mice, OX40L expression on OT-II OX40-KO donor T cells in OX40-KO recipient mice was clearly seen (Fig. 6*B*). These results indicate that the presence of OX40 down-regulates OX40L expression on T cells in vivo.

Next, to investigate the in vivo role of OX40L on T cell expansion, OT-II or OX40L-KO OT-II cells (Ly-5.2$^+$) were adoptively transferred into wild-type recipient mice (Ly-5.1$^+$), followed by the immunization of recipient mice with OVA/LPS. In a CFSE analysis, 4 days after transfer, in vivo cell division was similar in OT-II OX40L-KO T cells and OT-II T cells (Fig. 6*C*). Again, similarly to our in vitro data (Fig. 5*B*), OX40L-KO OT-II T cells, which can receive OX40 signals from OX40L expressed by recipient APCs, showed an impaired ability to survive for 10 days after stimulation (Fig. 6*D*). Collectively, OX40L on T cells contributes to T cell survival rather than early T cell expansion.

Finally, we performed an additional adoptive transfer experiment, in which OT-II or OX40L-KO OT-II T cells were transferred into sublethally irradiated congenic wild-type and OX40L-deficient mice. We then immunized the recipient mice with OVA emulsified in CFA. Four weeks after the immunization, OT-II OX40L-KO donor T cells showed significantly reduced numbers compared with OT-II donor T cells in both spleens and peripheral lymph nodes of recipient mice (Fig. 6*E*). Similarly, the absence of OX40L in recipient mice also appeared to suppress the survival of

of the 4-day cultures was measured as an indicator of cell proliferation and is expressed as the mean (±SD) of triplicate cultures. Similar results were obtained in at least four independent experiments. *D*, Purified CD4$^+$ T cells (5×10^4) from OT-II (■), OT-II OX40L-KO (△), and OT-II OX40-KO (□) mice were stimulated by irradiated OX40L-sufficient (wild-type) splenocytes (2×10^5) that were pulsed with 0.5 μM OVA peptide. At the different time points, [^{3}H]thymidine incorporation during the last 8 h of cultures was measured as an indicator of cell proliferation and is expressed as the mean (±SD) of triplicate cultures. Similar results were observed in three independent experiments. *E* and *F*, Purified CD4$^+$ T cells (5×10^4) from OT-II (■), OT-II OX40-KO (□), and OT-II OX40L-KO (△) mice, stimulated by either irradiated OX40L-deficient (*E*) or OX40L-sufficient (wild-type) (*F*) splenocytes (2×10^5) that were pulsed with various concentrations of OVA peptide [^{3}H]thymidine incorporation during the last 8 h of the 5-day cultures, were measured as an indicator of cell proliferation and expressed as the mean (±SD) of triplicate cultures. Similar results were observed in three independent experiments. *G*, Purified OT-II, OT-II OX40L-KO, and OT-II OX40-KO CD4$^+$ T cells were labeled with CFSE and stimulated by OVA-pulsed wild-type APCs. Ninety-six hours after stimulation, CFSE intensity of Vα2$^+$ CD4$^+$ T cells was estimated by flow cytometry. *Upper panels*, Show representatives of cell division patterns in three independent experiments. *Lower panels*, Demonstrate the mean ± SD of three independent experiments.

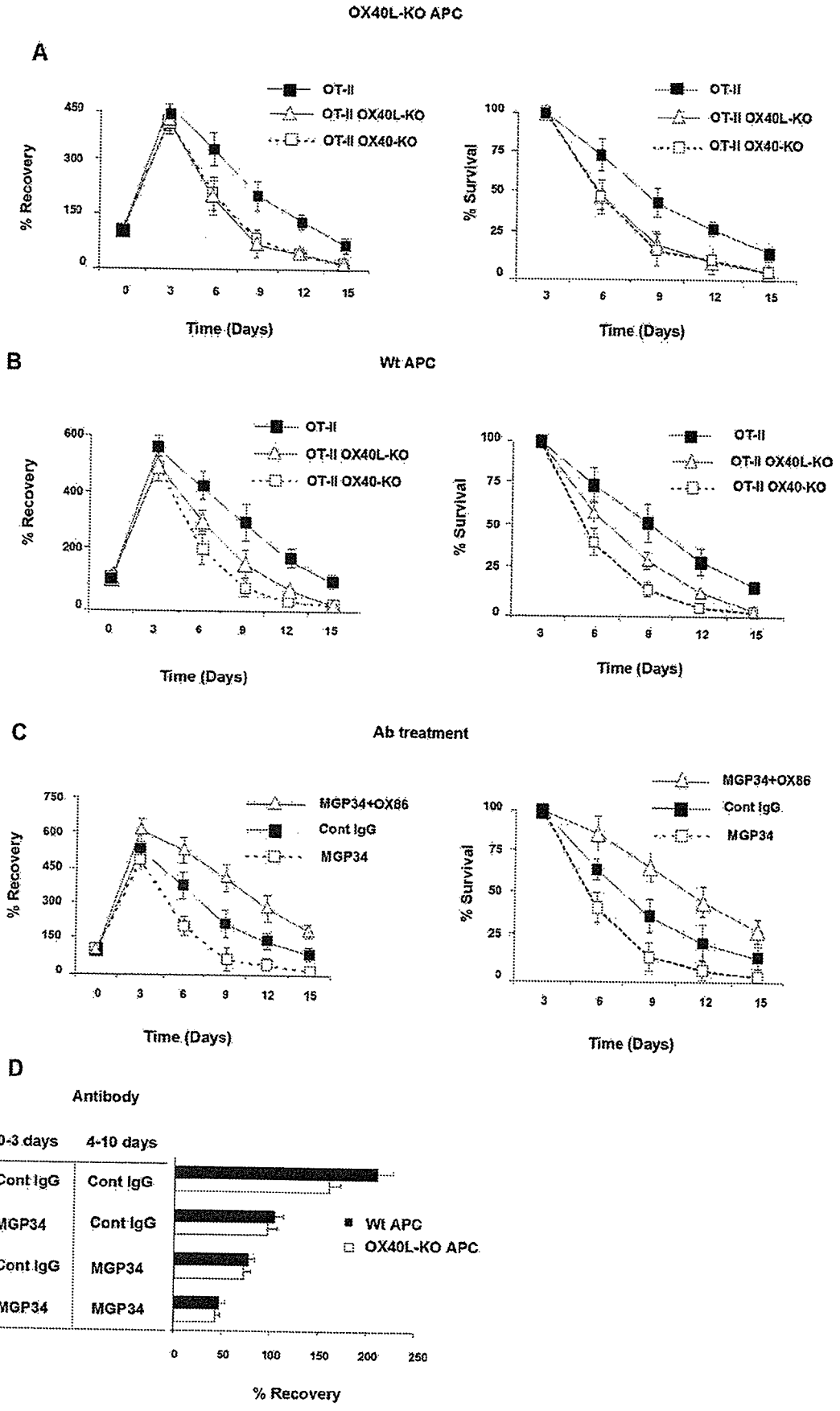
OX40L-KO APC
A
OT-II
OT-II OX40L-KO
OT-II OX40-KO
% Recovery
% Survival
Time (Days)
B
Wt APC
C
Ab treatment
MGP34+OX86
Cont IgG
MGP34
D
Antibody
0-3 days
4-10 days
Cont IgG
MGP34
Wt APC
OX40L-KO APC
% Recovery

transferred T cells (Fig. 6*E*). Indeed, the absence of OX40L both on the donor T cells and in the recipient mice had the most suppressive effect on donor T cell survival. All together, these results provide conclusive evidence that the OX40L on T cells, as well as the OX40L on APCs, contributes to the longevity of Ag-specific CD4 T cells.

Discussion

In the present study, we document a precise analysis of the expression and biological function of OX40L expressed on T cells. Using several conventional approaches, we show for the first time that activated CD4 T cells can intrinsically express OX40L both in vitro and in vivo. Although OX40L can also be transferred from OX40L-expressing cells to CD4 T cells (35), our results using OX40L-deficient APCs and recipient mice verified the endogenous expression of OX40L by T cells. We also demonstrated that the presence of the OX40 receptor on the same cell or adjacent cells suppresses the surface expression of OX40L on T cells. Several previous studies have described the expression of OX40L on activated T cells, such as Th1 cells and several CTL clones (18, 34). These studies, however, did not confirm whether the *OX40L* transcript was present in these T cells. Flow cytometric analysis by Kim et al. (34) demonstrated OX40L expression on Th1, but not Th2 cells. However, the OX40L-expressing Th1 cells had much lower OX40 expression than the Th2 cells, which had barely detectable levels of OX40L. Similarly, Fig. 1*A* demonstrates that PMA/ionomycin-treated T cells with higher OX40 expression level expressed less OX40L expression as compared with anti-CD3-treated T cells, which had lower level of OX40 expression. Based on our observations, we suggest that the insufficient expression of OX40 on Th1 cells and several CTL clones may have failed to suppress the surface OX40L expression, thus making it possible to detect OX40L on the Th1 cells. Further studies will be required to address the biological significance of the preferential OX40L expression on Th1 cells and CTL clones.

Regarding roles of OX40-OX40L interaction in CD4 T cell activation, when using polyclonal stimulation with anti-CD3 mAb (Fig. 4*A*), blockade of OX40 signals strongly suppressed early T cell proliferation (Fig. 4*A*). In contrast, upon stimulation with Ag peptide to naive OT-II T cells, OX40 signals are dispensable for early proliferation of T cells, but essential for T cell survival, as shown in Fig. 4*D* and previous reports (11, 34, 40, 41). We speculate that stronger TCR signals that may occur in TCR transgenic T cells upon Ag peptide stimulation might be enough for optimal early T cell proliferation even in the absence of OX40 signals. To clarify the precise mechanisms for these observations, further studies will be required.

The presence of OX40L on T cells encouraged us to undertake a more comprehensive analysis of its role in T cell responses. Accumulating evidence has demonstrated that OX40 signals control the frequency of effector CD4 T cells in late primary immune responses by promoting the survival and clonal expansion of T cells (7, 10, 11, 41). The present study has revealed that OX40L on T cells plays a major role in the survival of CD4 T cells that is associated with a significant increase in CD4 T cell proliferation. Given the findings of two previous papers that showed signals through OX40L induce c-*fos* expression and RANTES production in epithelial cell lines and endothelial cells, respectively (42, 43), it is tempting to speculate that downstream OX40L signals independently promote the proliferation and survival of T cells. However, our results indicated that the OX40 signals rather than the OX40L signals are critical for T cell survival (Fig. 4, *B* and *C*). In addition, we found that cross-linking OX40L on T cells with a recombinant soluble OX40 or anti-OX40L mAb did not promote T cell proliferation, but rather suppressed it (data not shown). These results strongly suggest that signals through OX40, but not OX40L, are essential for T cell proliferation and survival. Collectively, these data indicate that OX40L on T cells can initiate OX40 signals in adjacent T cells through direct T cell-T cell contact.

Analyzing CD4 T cell survival in vivo by transferring $CD4^+$ T cells into sublethally irradiated OX40L-sufficient or -deficient hosts clearly showed that OX40L expression is required on donor T cells for full-fledged T cell longevity (Fig. 6*E*). One previous report, however, demonstrated that adoptively transferred allogeneic OX40L-deficient T cells can successfully induce GVHD in OX40L-sufficient recipient mice in a pattern similar to that of wild-type T cells. By contrast, OX40L-KO recipient mice significantly suppressed the lethality of the GVHD following transfer of allogeneic wild-type T cells (23). These findings indicate that OX40 signals provided only by recipient APCs may be sufficient to induce graft-vs-host responses. Therefore, we speculate that the OX40L on T cells and APCs is used selectively in different types of immune responses. In contrast to little effect of OX40L deficiency on T cell in the GVHD model, deliberate OX40L expression on T cells in OX40L transgenic mice, which were constructed by using the mouse *lck* proximal promoter, demonstrated significant immunological abnormalities, such as production of autoantibodies, a marked increase in $CD4^+$ effector memory ($CD44^+CD62L^{low}$) T cell population, and spontaneous development of interstitial pneumonia and inflammatory bowel disease (44). Because excessive OX40 signals by using agonistic anti-OX40 mAb can break CD4 T cell tolerance (24, 45), deliberate OX40L expression on T cells in OX40L transgenic mice may be enough to induce autoimmunity.

We and others have demonstrated that OX40L expressed by APCs, such as DCs and activated B cells, can initiate OX40 signals in activated T cells (8, 9). Thus, the OX40-OX40L interaction has been thought to occur mainly during T cell-APC

FIGURE 5. OX40L expressed by T cells contributes to the long-term survival of CD4 T cells. *A* and *B*, Purified $CD4^+$ T cells (2×10^6) from wild-type OT-II (■), OX40-KO OT-II (□), and OX40L-KO-OT-II (△) mice were activated with OVA-pulsed OX40L-deficient (*A*) or OX40L-sufficient (wild-type) (*B*) APCs (1×10^7) in a six-well plate over 15 days. T cell recovery (*left panels*) and T cell survival (*right panels*) at the indicated days were assessed by excluding trypan blue-positive cells, and the calculation of the percentage of recovery was based on the input number of cells. Percentage of survival rate was calculated based on ratio (live cell number at the indicated day)/((peak) live cell number at day 3) × 100. In these figures, data are the average (±SD) of triplicate cultures, and similar results were obtained in at least three independent experiments. *C*, Purified wild-type OT-II $CD4^+$ T cells (2×10^6) were stimulated with OVA-pulsed irradiated OX40L-KO APCs (1×10^7) in the presence of control rat IgG (■; Cont IgG, 20 μg/ml), inhibitory anti-OX40L mAb (□; MGP34, 20 μg/ml), or MGP34 plus agonistic anti-OX40 mAb (OX86) (△; 10 μg/ml each), and cultured for 15 days. T cell recovery and survival at the indicated days were examined, as described. *D*, OT-II $CD4^+$ T cells (1×10^5) were stimulated by OVA-loaded OX40L-deficient (□) or OX40L-sufficient (wild-type) (■) APCs (4×10^5) over 10 days. Inhibitory anti-OX40L mAb (MGP34; 20 μg/ml) or control rat IgG (20 μg/ml) was added for 3 days starting at the beginning of the culture period. After being washed with PBS, cells were resuspended in complete medium and cultured an additional 7 days in the presence of either control IgG or MGP 34. Ten days later, the percentage of survival was calculated. Similar results were obtained in two independent experiments.

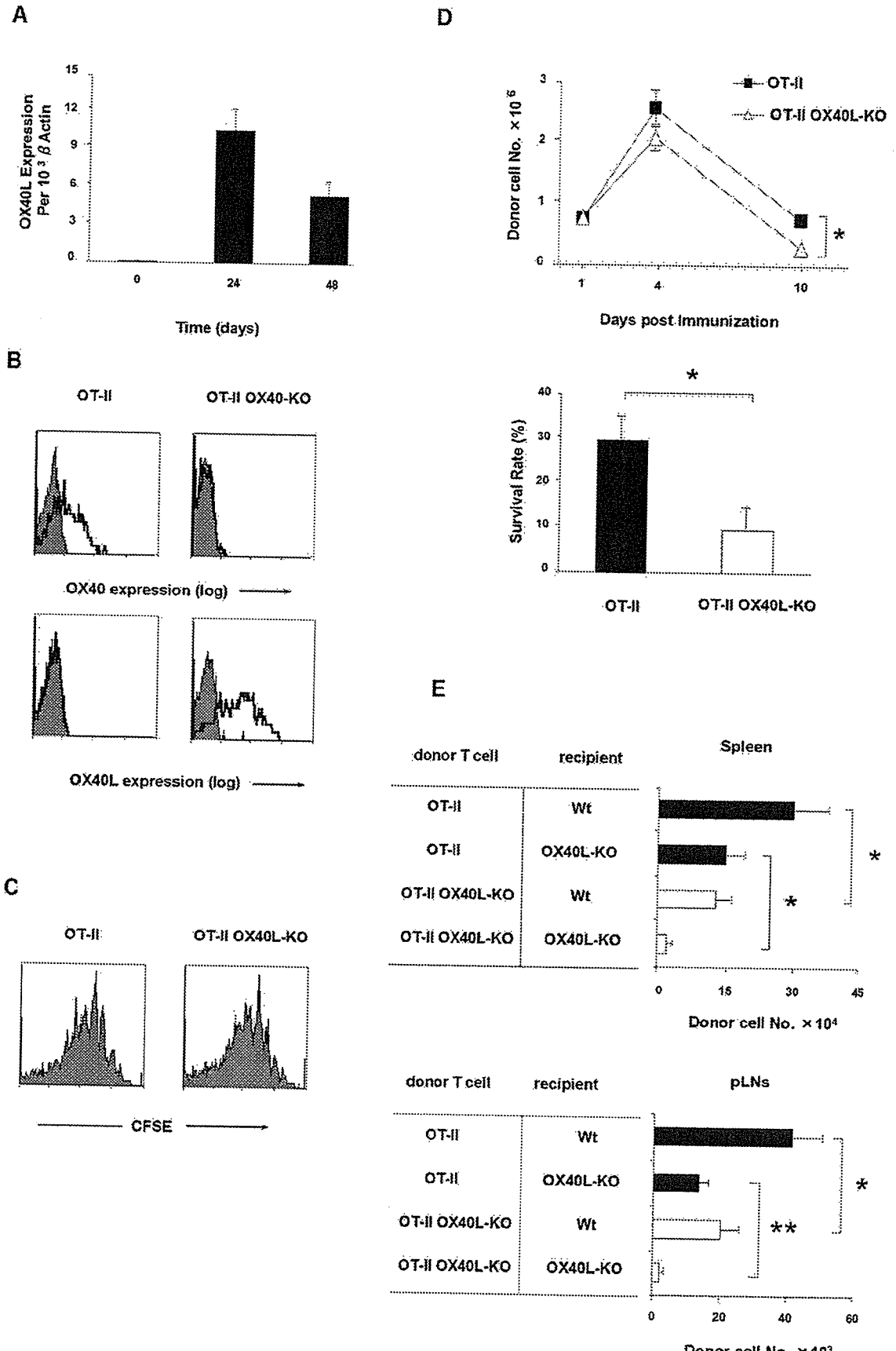

FIGURE 6. OX40L on donor T cells supports their survival after Ag stimulation in vivo. *A*, Purified $CD4^+$ T cells (1×10^7) from Ly-5.2^+ OT-II TCR transgenic mice were transferred into wild-type (non-OT-II) Ly-5.1^+ mice. Twenty-four hours later, each recipient mouse was immunized i.v. with 2 mg of OVA plus 50 μg of LPS. At the indicated time after immunization, the donor Ly-5.2^+ T cells were magnetically isolated (*Figure legend continues*)

interaction. However, OX40 expression on naive CD4 T cells peaks 2–3 days after Ag stimulation (6) and continues at least up to 15 days after the stimulation (Fig. 3*B*). Recently, intravital two-photon imaging of CD4 T cell behavior in the lymph nodes showed that the naive CD4 T cell-DC interaction lasts 24–48 h after Ag priming (46, 47), and about one-half of the Ag-specific T cells leave DCs near high endothelial venules and move into the T cell area in the deep paracortex of lymph nodes (48). These findings support the idea that OX40L expressed by cells different from DCs may also be involved in OX40-OX40L interactions. Our in vitro results (Fig. 2*D*) demonstrate that OX40L on T cells binds to OX40 on T cells through T cell-T cell contact. In addition, the in vivo results shown in Fig. 6 suggest functional roles for OX40-OX40L binding during T cell-T cell interactions in T cell survival. Although previous studies suggest that OX40L on $CD4^+CD3^-$ accessory cells (49) and B cells (50) can costimulate $OX40^+$ CD4 T cells, the in vivo roles for the OX40L expression on these cells in supporting CD4 T cell survival are unclear. We have hypothesized that the accumulation of Ag-experienced T cells in the T cell zone of the secondary lymphoid organs may be conducted by OX40-OX40L interactions through direct T cell-T cell cross talk. Moreover, the sustained expression levels of OX40 and OX40L on activated T cells (Fig. 3*B*) suggest that, after the T cells and APCs (DCs) separate, T cells may still support OX40 signals in an autocrine or paracrine manner. Considering all of the available evidence, we conclude that OX40L expressed by CD4 T cells can provide autonomous OX40 signals through T cell-T cell interactions that contribute to the longevity of Ag-specific CD4 T cells and lead to the generation and survival of CD4 memory T cells.

Acknowledgments

We thank Dr. Ndhlovu for the critical reading and Dr. Murata for the excellent technique.

Disclosures

The authors have no financial conflict of interest.

References

1. Mueller, D. L., M. K. Jenkins, and R. H. Schwartz. 1989. Clonal expansion versus functional clonal inactivation: a costimulatory signalling pathway determines the outcome of T cell antigen receptor occupancy. *Annu. Rev. Immunol.* 7: 445–480.
2. Lenschow, D. J., T. L. Walunas, and J. A. Bluestone. 1996. CD28/B7 system of T cell costimulation. *Annu. Rev. Immunol.* 14: 233–258.
3. Croft, M. 2003. Co-stimulatory members of the TNFR family: keys to effective T-cell immunity? *Nat. Rev. Immunol.* 3: 609–620.
4. Watts, T. H. 2005. TNF/TNFR family members in costimulation of T cell responses. *Annu. Rev. Immunol.* 23: 23–68.
5. Sugamura, K., N. Ishii, and A. D. Weinberg. 2004. Therapeutic targeting of the effector T-cell co-stimulatory molecule OX40. *Nat. Rev. Immunol.* 4: 420–431.
6. Gramaglia, I., A. D. Weinberg, M. Lemon, and M. Croft. 1998. Ox-40 ligand: a potent costimulatory molecule for sustaining primary CD4 T cell responses. *J. Immunol.* 161: 6510–6517.
7. Kopf, M., C. Ruedl, N. Schmitz, A. Gallimore, K. Lefrang, B. Ecabert, B. Odermatt, and M. F. Bachmann. 1999. OX40-deficient mice are defective in Th cell proliferation but are competent in generating B cell and CTL responses after virus *Infect. Immun.* 11: 699–708.
8. Chen, A. I., A. J. McAdam, J. E. Buhlmann, S. Scott, M. L. Lupher, Jr., E. A. Greenfield, P. R. Baum, W. C. Fanslow, D. M. Calderhead, G. J. Freeman, and A. H. Sharpe. 1999. Ox40-ligand has a critical costimulatory role in dendritic cell:T cell interactions. *Immunity* 11: 689–698.
9. Murata, K., N. Ishii, H. Takano, S. Miura, L. C. Ndhlovu, M. Nose, T. Noda, and K. Sugamura. 2000. Impairment of antigen-presenting cell function in mice lacking expression of OX40 ligand. *J. Exp. Med.* 191: 365–374.
10. Gramaglia, I., A. Jember, S. D. Pippig, A. D. Weinberg, N. Killeen, and M. Croft. 2000. The OX40 costimulatory receptor determines the development of CD4 memory by regulating primary clonal expansion. *J. Immunol.* 165: 3043–3050.
11. Rogers, P. R., J. Song, I. Gramaglia, N. Killeen, and M. Croft. 2001. OX40 promotes Bcl-x_L and Bcl-2 expression and is essential for long-term survival of CD4 T cells. *Immunity* 15: 445–455.
12. Hendriks, J., Y. Xiao, J. W. Rossen, K. F. van der Sluijs, K. Sugamura, N. Ishii, and J. Borst. 2005. During viral infection of the respiratory tract, CD27, 4-1BB, and OX40 collectively determine formation of $CD8^+$ memory T cells and their capacity for secondary expansion. *J. Immunol.* 175: 1665–1676.
13. Stuber, E., M. Neurath, D. Calderhead, H. P. Fell, and W. Strober. 1995. Cross-linking of OX40 ligand, a member of the TNF/NGF cytokine family, induces proliferation and differentiation in murine splenic B cells. *Immunity* 2: 507–521.
14. Imura, A., T. Hori, K. Imada, T. Ishikawa, Y. Tanaka, M. Maeda, S. Imamura, and T. Uchiyama. 1996. The human OX40/gp34 system directly mediates adhesion of activated T cells to vascular endothelial cells. *J. Exp. Med.* 183: 2185–2195.
15. Ohshima, Y., Y. Tanaka, H. Tozawa, Y. Takahashi, C. Maliszewski, and G. Delespesse. 1997. Expression and function of OX40 ligand on human dendritic cells. *J. Immunol.* 159: 3838–3848.
16. Pippig, S. D., C. Pena-Rossi, J. Long, W. R. Godfrey, D. J. Fowell, S. L. Reiner, M. L. Birkeland, R. M. Locksley, A. N. Barclay, and N. Killeen. 1999. Robust B cell immunity but impaired T cell proliferation in the absence of CD134 (OX40). *J. Immunol.* 163: 6520–6529.
17. Weinberg, A. D., K. W. Wegmann, C. Funatake, and R. H. Whitham. 1999. Blocking OX-40/OX-40 ligand interaction in vitro and in vivo leads to decreased T cell function and amelioration of experimental allergic encephalomyelitis. *J. Immunol.* 162: 1818–1826.
18. Takasawa, N., N. Ishii, N. Higashimura, K. Murata, Y. Tanaka, M. Nakamura, T. Sasaki, and K. Sugamura. 2001. Expression of gp34 (OX40 ligand) and OX40 on human T cell clones. *Jpn. J. Cancer Res.* 92: 377–382.
19. Wang, H. C., and J. R. Klein. 2001. Multiple levels of activation of murine $CD8^+$ intraepithelial lymphocytes defined by OX40 (CD134) expression: effects on cell-mediated cytotoxicity, IFN-γ, and IL-10 regulation. *J. Immunol.* 167: 6717–6723.
20. Sato, T., N. Ishii, K. Murata, K. Kikuchi, S. Nakagawa, L. C. Ndhlovu, and K. Sugamura. 2002. Consequences of OX40-OX40 ligand interactions in Langerhans cell function: enhanced contact hypersensitivity responses in OX40L-transgenic mice. *Eur. J. Immunol.* 32: 3326–3335.

(purity, >90%) from the spleen of recipient mice, and the total RNA was extracted from the purified donor T cells. Relative *OX40L* expression was quantified using real-time PCR, as described in Fig. 1*B*. *B*, Purified $CD4^+$ T cells (1×10^7) from $Ly\text{-}5.1^+$ OT-II and OT-II OX40-KO mice were transferred into congenic ($Ly\text{-}5.2^+$) wild-type or OX40-KO mice. Twenty-four hours later, each recipient mouse was immunized i.p. with 50 μg of OVA peptide emulsified in CFA. Three days after immunization, the OX40 and OX40L expression on donor $Ly\text{-}5.1^+$ T cells was examined by flow cytometry. Filled histograms represent control staining. *C*, Purified $CD4^+$ T cells (5×10^6) from $Ly\text{-}5.2^+$ OT-II or $Ly\text{-}5.2^+$ OX40L-KO OT-II mice were labeled with CFSE and transferred into wild-type $Ly\text{-}5.1^+$ mice, and recipient mice were then immunized with OVA plus LPS. Splenocytes were harvested 4 days after immunization, and dilution of CFSE fluorescence intensity of donor T cells was analyzed by FACS. Representative results of two independent experiments were shown. *D*, Purified $CD4^+$ T cells (1×10^7) from $Ly\text{-}5.2^+$ OT-II or $Ly\text{-}5.2^+$ OX40L-KO OT-II mice were transferred into wild-type $Ly\text{-}5.1^+$ mice, and recipient mice were then immunized with OVA plus LPS. Spleen cells of the recipient mice were harvested 1, 4, and 10 days after Ag administration; stained for Ly-5.2, TCR-Vα2, and TCR-Vβ5.1; and analyzed by flow cytometry. The absolute number of donor T cells in the spleen of recipient mice (*upper*) and survival rate of donor T cells (*lower*) are shown. Percentage of survival rate was calculated based on ratio (donor T cell number at day 10)/(donor T cell number at day 4) × 100. Results represent the mean ± SD from three mice per group, and are representative of two independent experiments. The significance of the data was evaluated by Student's *t* test (*, represents $p < 0.01$). *E*, Purified $CD4^+$ T cells (2.5×10^6) from $Ly\text{-}5.1^+$ OT-II (■) or OX40L-KO OT-II (□) mice were transferred to sublethally irradiated (500 cGy) congenic (Ly-5.2) wild-type or OX40L-deficient mice. One day later, recipient mice were immunized with OVA peptide emulsified in CFA. Spleens (*upper panel*) and peripheral (inguinal and mesenteric) lymph nodes (pLNs, *lower panel*) were extracted 4 wk after immunization, and the cells were stained for $Ly\text{-}5.1^+$, TCR-Vα2, and TCR-Vβ5.1. The number of surviving donor ($Ly\text{-}5.1^+$ TCR-$V\alpha2^+$ TCR-$V\beta5.1^+$) T cells was calculated by microscopic cell count and flow cytometric analysis. Results represent the mean ± SD from five mice per group. The significance of the data was evaluated by Student's *t* test (* and **, represent $p < 0.01$ and $p < 0.001$, respectively).

21. Miura, S., K. Ohtani, N. Numata, M. Niki, K. Ohbo, Y. Ina, T. Gojobori, Y. Tanaka, H. Tozawa, M. Nakamura, et al. 1991. Molecular cloning and characterization of a novel glycoprotein, gp34, that is specifically induced by the human T-cell leukemia virus type I transactivator p40tax. *Mol. Cell. Biol.* 11: 1313–1325.
22. Ndhlovu, L. C., N. Ishii, K. Murata, T. Sato, and K. Sugamura. 2001. Critical involvement of OX40 ligand signals in the T cell priming events during experimental autoimmune encephalomyelitis. *J. Immunol.* 167: 2991–2999.
23. Blazar, B. R., A. H. Sharpe, A. I. Chen, A. Panoskaltsis-Mortari, C. Lees, H. Akiba, H. Yagita, N. Killeen, and P. A. Taylor. 2003. Ligation of OX40 (CD134) regulates graft-versus-host disease (GVHD) and graft rejection in allogeneic bone marrow transplant recipients. *Blood* 101: 3741–3748.
24. Takeda, I., S. Ine, N. Killeen, L. C. Ndhlovu, K. Murata, S. Satomi, K. Sugamura, and N. Ishii. 2004. Distinct roles for the OX40-OX40 ligand interaction in regulatory and nonregulatory T cells. *J. Immunol.* 172: 3580–3589.
25. Hathcock, K. S., G. Laszlo, C. Pucillo, P. Linsley, and R. J. Hodes. 1994. Comparative analysis of B7-1 and B7-2 costimulatory ligands: expression and function. *J. Exp. Med.* 180: 631–640.
26. Hakamada-Taguchi, R., T. Kato, H. Ushijima, M. Murakami, T. Uede, and H. Nariuchi. 1998. Expression and co-stimulatory function of B7-2 on murine $CD4^+$ T cells. *Eur. J. Immunol.* 28: 865–873.
27. Azuma, M., H. Yssel, J. H. Phillips, H. Spits, and L. L. Lanier. 1993. Functional expression of B7/BB1 on activated T lymphocytes. *J. Exp. Med.* 177: 845–850.
28. Jeannin, P., N. Herbault, Y. Delneste, G. Magistrelli, S. Lecoanet-Henchoz, G. Caron, J. P. Aubry, and J. Y. Bonnefoy. 1999. Human effector memory T cells express CD86: a functional role in naive T cell priming. *J. Immunol.* 162: 2044–2048.
29. Brugnoni, D., P. Airo, R. Marino, L. D. Notarangelo, R. A. van Lier, and R. Cattaneo. 1997. CD70 expression on T-cell subpopulations: study of normal individuals and patients with chronic immune activation. *Immunol. Lett.* 55: 99–104.
30. Wagner, D. H., Jr., G. Vaitaitis, R. Sanderson, M. Poulin, C. Dobbs, and K. Haskins. 2002. Expression of CD40 identifies a unique pathogenic T cell population in type 1 diabetes. *Proc. Natl. Acad. Sci. USA* 99: 3782–3787.
31. Bourgeois, C., B. Rocha, and C. Tanchot. 2002. A role for CD40 expression on $CD8^+$ T cells in the generation of $CD8^+$ T cell memory. *Science* 297: 2060–2063.
32. Tesselaar, K., Y. Xiao, R. Arens, G. M. van Schijndel, D. H. Schuurhuis, R. E. Mebius, J. Borst, and R. A. van Lier. 2003. Expression of the murine CD27 ligand CD70 in vitro and in vivo. *J. Immunol.* 170: 33–40.
33. Baum, P. R., R. B. Gayle III, F. Ramsdell, S. Srinivasan, R. A. Sorensen, M. L. Watson, M. F. Seldin, K. N. Clifford, K. Grabstein, M. R. Alderson, et al. 1994. Identification of OX40 ligand and preliminary characterization of its activities on OX40 receptor. *Circ. Shock* 44: 30–34.
34. Kim, M. Y., V. Bekiaris, F. M. McConnell, F. M. Gaspal, C. Raykundalia, and P. J. Lane. 2005. OX40 signals during priming on dendritic cells inhibit CD4 T cell proliferation: IL-4 switches off OX40 signals enabling rapid proliferation of Th2 effectors. *J. Immunol.* 174: 1433–1437.
35. Baba, E., Y. Takahashi, J. Lichtenfeld, R. Tanaka, A. Yoshida, K. Sugamura, N. Yamamoto, and Y. Tanaka. 2001. Functional CD4 T cells after intercellular molecular transfer of OX40 ligand. *J. Immunol.* 167: 875–883.
36. Biagi, E., G. Dotti, E. Yvon, E. Lee, M. Pule, S. Vigouroux, S. Gottschalk, U. Popat, R. Rousseau, and M. Brenner. 2005. Molecular transfer of CD40 and OX40 ligands to leukemic human B cells induces expansion of autologous tumor-reactive cytotoxic T lymphocytes. *Blood* 105: 2436–2442.
37. Bamden, M. J., J. Allison, W. R. Heath, and F. R. Carbone. 1998. Defective TCR expression in transgenic mice constructed using cDNA-based α- and β-chain genes under the control of heterologous regulatory elements. *Immunol. Cell Biol.* 76: 34–40.
38. Ishii, N., T. Takeshita, Y. Kimura, K. Tada, M. Kondo, M. Nakamura, and K. Sugamura. 1994. Expression of the IL-2 receptor γ chain on various populations in human peripheral blood. *Int. Immunol.* 6: 1273–1277.
39. Oshima, Y., L. P. Yang, T. Uchiyama, Y. Tanaka, P. Baum, M. Sergerie, P. Hermann, and G. Delespesse. 1998. OX40 costimulation enhances interleukin-4 (IL-4) expression at priming and promotes the differentiation of naive human $CD4^+$ T cells into high IL-4-producing effectors. *Blood* 92: 3338–3345.
40. Song, J., S. Salek-Ardakani, P. R. Rogers, M. Cheng, L. Van Parijs, and M. Croft. 2004. The costimulation-regulated duration of PKB activation controls T cell longevity. *Nat. Immunol.* 5: 150–158.
41. Song, J., T. So, M. Cheng, X. Tang, and M. Croft. 2005. Sustained survivin expression from OX40 costimulatory signals drives T cell clonal expansion. *Immunity* 22: 621–631.
42. Kotani, A., T. Hori, Y. Matsumura, and T. Uchiyama. 2002. Signaling of gp34 (OX40 ligand) induces vascular endothelial cells to produce a CC chemokine RANTES/CCL5. *Immunol. Lett.* 84: 1–7.
43. Matsumura, Y., T. Hori, S. Kawamata, A. Imura, and T. Uchiyama. 1999. Intracellular signaling of gp34, the OX40 ligand: induction of *c-jun* and *c-fos* mRNA expression through gp34 upon binding of its receptor, OX40. *J. Immunol.* 163: 3007–3011.
44. Murata, K., M. Nose, L. C. Ndhlovu, T. Sato, K. Sugamura, and N. Ishii. 2002. Constitutive OX40/OX40 ligand interaction induces autoimmune-like diseases. *J. Immunol.* 169: 4628–4636.
45. Bansal-Pakala, P., A. G. Jember, and M. Croft. 2001. Signaling through OX40 (CD134) breaks peripheral T-cell tolerance. *Nat. Med.* 7: 907–912.
46. Miller, M. J., O. Safrina, I. Parker, and M. D. Cahalan. 2004. Imaging the single cell dynamics of $CD4^+$ T cell activation by dendritic cells in lymph nodes. *J. Exp. Med.* 200: 847–856.
47. Mempel, T. R., S. E. Henrickson, and U. H. Von Andrian. 2004. T-cell priming by dendritic cells in lymph nodes occurs in three distinct phases. *Nature* 427: 154–159.
48. Shakhar, G., R. L. Lindquist, D. Skokos, D. Dudziak, J. H. Huang, M. C. Nussenzweig, and M. L. Dustin. 2005. Stable T cell-dendritic cell interactions precede the development of both tolerance and immunity in vivo. *Nat. Immunol.* 6: 707–714.
49. Kim, M. Y., F. M. Gaspal, H. E. Wiggett, F. M. McConnell, A. Gulbranson-Judge, C. Raykundalia, L. S. Walker, M. D. Goodall, and P. J. Lane. 2003. $CD4^+CD3^-$ accessory cells costimulate primed CD4 T cells through OX40 and CD30 at sites where T cells collaborate with B cells. *Immunity* 18: 643–654.
50. Linton, P. J., B. Bautista, E. Biederman, E. S. Bradley, J. Harbertson, R. M. Kondrack, R. C. Padrick, and L. M. Bradley. 2003. Costimulation via OX40L expressed by B cells is sufficient to determine the extent of primary CD4 cell expansion and Th2 cytokine secretion in vivo. *J. Exp. Med.* 197: 875–883.

Available online at www.sciencedirect.com
SCIENCE DIRECT
ELSEVIER
Biochemical and Biophysical Research Communications 341 (2006) 391–398
BBRC
www.elsevier.com/locate/ybbrc

Application of HSVtk suicide gene to X-SCID gene therapy: Ganciclovir treatment offsets gene corrected X-SCID B cells

Toru Uchiyama [a], Satoru Kumaki [a,*], Yoshinori Ishikawa [b], Masafumi Onodera [c], Miki Sato [a], Wei Du [a], Yoji Sasahara [a], Nobuyuki Tanaka [b], Kazuo Sugamura [b], Shigeru Tsuchiya [a]

[a] *Department of Pediatric Oncology, Institute of Development, Aging and Cancer, Tohoku University, Seiryo-machi 4-1, Aoba-ku, Sendai 980-8575, Japan*
[b] *Department of Microbiology and Immunity, Graduate School of Medicine, Tohoku University, Seiryo-machi 2-1, Aoba-ku, Sendai 980-8575, Japan*
[c] *Major of Medical Sciences, Graduate School of Comprehensive Human Sciences, Tsukuba University, Tennodai 1-1-1, Tsukuba 305-8575, Japan*

Received 28 December 2005
Available online 11 January 2006

Abstract

Recently, a serious adverse effect of uncontrolled clonal T cell proliferation due to insertional mutagenesis of retroviral vector was reported in X-SCID gene therapy clinical trial. To offset the side effect, we have incorporated a suicide gene into therapeutic retroviral vector for selective elimination of transduced cells. In this study, B-cell lines from two X-SCID patients were transduced with bicistronic retroviral vector carrying human γc chain cDNA and Herpes simplex virus thymidine kinase gene. After confirmation of functional reconstitution of the γc chain, the cells were treated with ganciclovir (GCV). The γc chain positive cells were eliminated under low concentration without cytotoxicity on untransduced cells and have not reappeared at least for 5 months. Furthermore, the γc chain transduced cells were still sensitive to GCV after five months. These results demonstrated the efficacy of the suicide gene therapy although further in vivo studies are required to assess feasibility of this approach in clinical trial.

Keywords: Gene therapy; X-SCID; γc chain; Retroviral vector; Suicide gene; HSVtk

X-linked severe combined immunodeficiency (X-SCID) is a disease characterized by the absence of humoral and cellular immunity due to mutations in the gene encoding the common gamma (γc) chain [1,2]. The γc chain is an essential component of the cytokine receptors for the interleukins 2, 4, 7, 9, 15, and 21 [3–5]. Cytokine signals through the γc chain are required for differentiation and proliferation of T cells, NK cells, and functional B cells, and abnormal signaling through the receptor results in the immunological defects. The X-SCID patients are at risk of severe, recurrent infections unless stem cell transplantation is performed [2]. The overall survival of X-SCID patients who received allogeneic bone marrow transplantation (BMT) from an HLA-identical sibling is more than 90% [6]. However, if a patient does not have a well-matched family donor, survival rate is ranging from 50% to 78%, owing to potential risks of severe complications such as graft-versus-host disease (GVHD), graft rejection, and slow T cell development [7,8].

Clinical trial of X-SCID gene therapy was initiated in France from 1999 [9]. Ten patients with typical X-SCID were treated between 1999 and 2002, and T cell reconstitution was observed in 9 out of 10 cases resulting in clinical benefits such as resolution of ongoing infections and leaving their protected environments [2,10]. In addition, most of the patients showed NK cell recovery and immunoglobulin production [2,9,10]. Similar results were observed in four patients treated by retrovirus-based gene therapy in England [11]. Overall, gene therapy is very efficient in correcting immunodeficiency.

* Corresponding author. Fax: +81 22 717 8495.
E-mail address: kumakis@idac.tohoku.ac.jp (S. Kumaki).

0006-291X/$ - see front matter © 2006 Elsevier Inc. All rights reserved.
doi:10.1016/j.bbrc.2005.12.199

However, clonal T cell proliferation occurred in three out of eleven patients treated in France [12,13]. The primary cause was insertion of the provirus within the *LMO2* locus, leading to aberrant expression of LMO-2 in mature T cells and thereby uncontrolled proliferation. Aberrant LMO-2 expression is associated with a form of T cell acute leukemia in childhood [14]. In addition, a retrovirus-induced mouse lymphoma that contained insertions in both *LMO2* and *IL2RG* was reported [15]. Recently, myeloid sarcoma was observed in a non-human primate associated with a retrovirus vector insertion [16]. Although retrovirus-based gene therapy has shown promising results in correcting immunodeficiency, the risk and consequences of insertional mutagenesis by retroviral vector must be taken into consideration. One of the alternatives is to incorporate a suicide gene into a therapeutic retroviral vector to eliminate the lymphoproliferative disease due to insertional mutagenesis. The Herpes simplex virus thymidine kinase (HSVtk) gene in combination with ganciclovir (GCV) has been used in clinical trials to control T cell mediated GVHD after hematopoietic stem cell transplantation [17–19] and cancer gene therapies [20–22]. In this study, we demonstrated functional expression of the γc chain after the bicistronic retrovirus-mediated gene transfer and importantly, the selective elimination of γc chain positive cells after GCV treatment for a period of 5 months.

Materials and methods

X-SCID patients' B lines. Peripheral blood mononuclear cells (PBMCs) were obtained from two X-SCID patients with written informed consent. The cells were transformed with Epstein-Barr virus (EBV)-containing supernatant to establish B-cell lines as previously described [23]. Both patients had typical clinical presentation of X-SCID, and the patient 2 was described previously [24]. The laboratory findings of patient 1 revealed absence of own T cells and NK cells, and profound hypogammaglobulinemia despite normal numbers of B cells. Mutations in the γc chain of the patients are shown in Table 1. Sequencing analysis of the γc chain was performed according to the standard method [25].

Retrovirus vector and producing cell lines. The entire human γc chain cDNA was generated by polymerase chain reaction (PCR) from γc chain expression vector, pSRG1 [4]. The upstream primer 5′-CATTAGCGGC CGCGAAGAGCAAGCGCCATGTTG-3′ and the downstream primer 5′-GCCGCGGATCCGATGATTATCAACAGAAACT-3′ contain *Not*I and *Bam*HI sites, respectively. The HSVtk cDNA was generated by PCR from a retroviral vector SFCMM3 encompassing an HSVtk gene [18]. The upstream primer 5′-GAATTCGTTGATCCGCCGCCACCATGG-3′ and the downstream primer 5′-GAAGCGCATCGATCCTCGAGTTAAT TCTCAG-3′ contain *Nco*I and *Cla*I sites, respectively. The backbone vector pDΔNsamIRESEGFP, with intact splice donor and splice acceptor sequences for generation of subgenomic mRNA, has a long-terminal repeat (LTR) derived from Murine stem cell virus (MSCV). The enhanced green fluorescent protein (EGFP) cDNA is located downstream of the internal ribosome entry site (IRES) of the backbone vector. The EGFP fragment was excised from pDΔNsamIRESEGFP using *Nco*I and *Cla*I sites, and replaced by the HSVtk gene. The γc chain cDNA was inserted into the vector using *Not*I and *Bam*HI sites. MSCV LTR promoter of the resultant bicistronic vector, pD-γc/TK, drives the expression of both the γc chain and HSVtk genes simultaneously. The pD-γc/TK vector was co-transfected with VSV-G plasmid encoding the Vesicular stomatitis virus G glycoprotein into 293gp cells which were stably expressing transfected MoMLV *gag* and *pol* genes [26]. Conditioned medium from the transfected 293gp cells was collected, filtered, and used for transduction of the gibbon ape leukemia virus (GALV)-pseudotyped MoMLV producing cell line PG13 [27]. After expansion of the transduced PG13 cells for 96 h, the cells were stained with a PE-conjugated anti-human γc chain monoclonal antibody, TUGh4 (BD Bioscience, San Diego, CA) and analyzed by FACSCalibur (Becton Dickinson, San Jose, CA) as previously described [25]. The γc chain positive cells were enriched by magnetic sorting using anti-PE micro beads and Auto-MACS (Miltenyi Biotec, Germany).

Transduction of EBV-transformed BCLs from X-SCID patients. EBV-transformed BCLs established from two typical X-SCID patients were infected by co-culturing with irradiated (30 Gy) producer cells in the presence of 8 μg/ml protamine sulfate. Cells were infected for two cycles each lasting 48 h.

IL-2 induced Jak3 phosphorylation. The EBV-transformed BCLs were cultured in serum-free RPMI 1640 for 24 h in humidified 5% CO_2 at 37 °C. After washing, the cells were stimulated by addition of 100 ng/ml IL-2 for 15 min at 37 °C. Stimulated cells were centrifuged and then lysed in ice-cold buffer (50 mM Tris–HCl, 10 mM EDTA, 100 mM NaF, 10 mM sodium pyrophosphate decahydrate, 10 mM sodium molybdate, 2 mM sodium orthovanadate, 2 mM PMSF, and 0.1% aprotinin). For Jak3 phosphorylation analysis, lysates were clarified by centrifugation and immunoprecipitated with a polyclonal antibody against Jak3 protein (Santa Cruz Biotechnology, Santa Cruz, CA). Bound proteins were resolved by SDS–PAGE and transferred to nitrocellulose membrane. The membrane was blotted with a monoclonal antibody against phosphotyrosine, 4G10 (Upstate Biotechnology, Lake Placid, NY). Bound primary antibodies were detected by the horseradish peroxidase-conjugated anti-mouse IgG antibody followed by enhanced chemiluminescence (ECL) detection reagent.

Sensitivity of transduced cells to GCV in vitro. The γc chain transduced BCLs were plated in 48-well plates at a density of 1×10^5 cells/well. The cells were treated with 0.1, 1.0, 10, 25, 50, and 100 μM GCV for 14 days. Control cells (without GCV) were grown under the same condition. Percentages of the γc chain positive cells were assessed by flow cytometric analysis, every two days for 18 days after addition of GCV.

Cell proliferation and viability. Non-transduced BCLs were treated with various concentrations (1.0, 10, 25, 50, and 100 μM) of GCV. The total cell numbers were counted each day for 7 days. Cell viability was evaluated by trypan blue staining simultaneously. The percentages of viable cells were average viability of three independent experiments' scoring of 100 cells.

Table 1
Characterization of γc mutations in patients

Patient No.	Mutated exon	Nucleotide alteration	Protein alteration	TUGh4 staining
1	3	336T → C	S108P	—
2	6	868G → A	R285Q	—

Results

Retrovirus vector mediated expression of γc chain

To generate the recombinant retroviral vector pD-γc/TK, a full-length human γc chain cDNA and the HSVtk gene were cloned into *Not*I/*Bam*HI and *Nco*I/*Cla*I sites of pDΔNsamIRESEGFP, respectively (Fig. 1). pD-γc/TK was co-transfected with VSV-G plasmid encoding the vesicular stomatitis virus G glycoprotein into 293gp cells. Subsequently, 293gp-derived retroviral vector supernatants were used to transduce PG13 GALV-pseudotyped packaging cells. Four days later, the γc chain positive PG13 cells

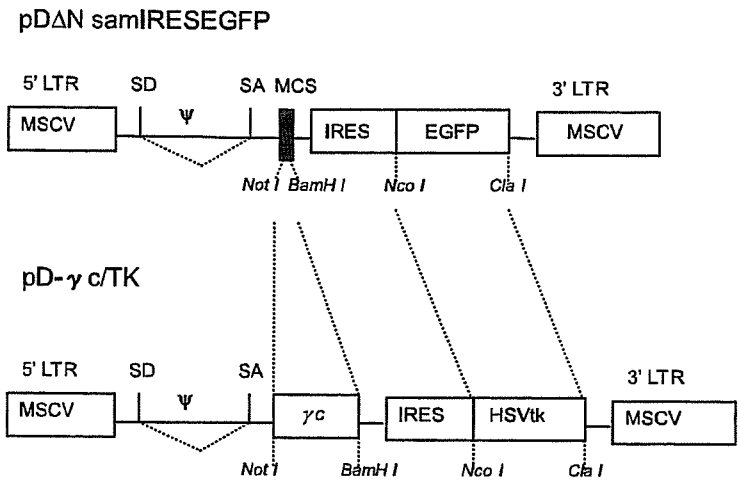

Fig. 1. Schematic representation of the pD-γc/TK vector. The backbone vector pDΔNsamIRESEGFP contains MSCV LTR with intact splice donor and splice acceptor sequences. The γc chain cDNA was inserted into multiple cloning sites (MCS) and EGFP fragment was replaced with the HSVtk gene. Characteristic sequences present in each vector are abbreviated as follows: ψ, packaging signal; MCS, multiple cloning sites; SD, splice donor; and SA, splice acceptor.

were sorted by Auto-MACS, and more than 90% of the sorted cells expressed the γc chain on the cell surface (data not shown). The resultant virus-producing PG13 cells were co-cultured with BCLs established from two typical X-SCID patients (P1 and P2). Clinical profiles and mutational analysis of the X-SCID patients are described in

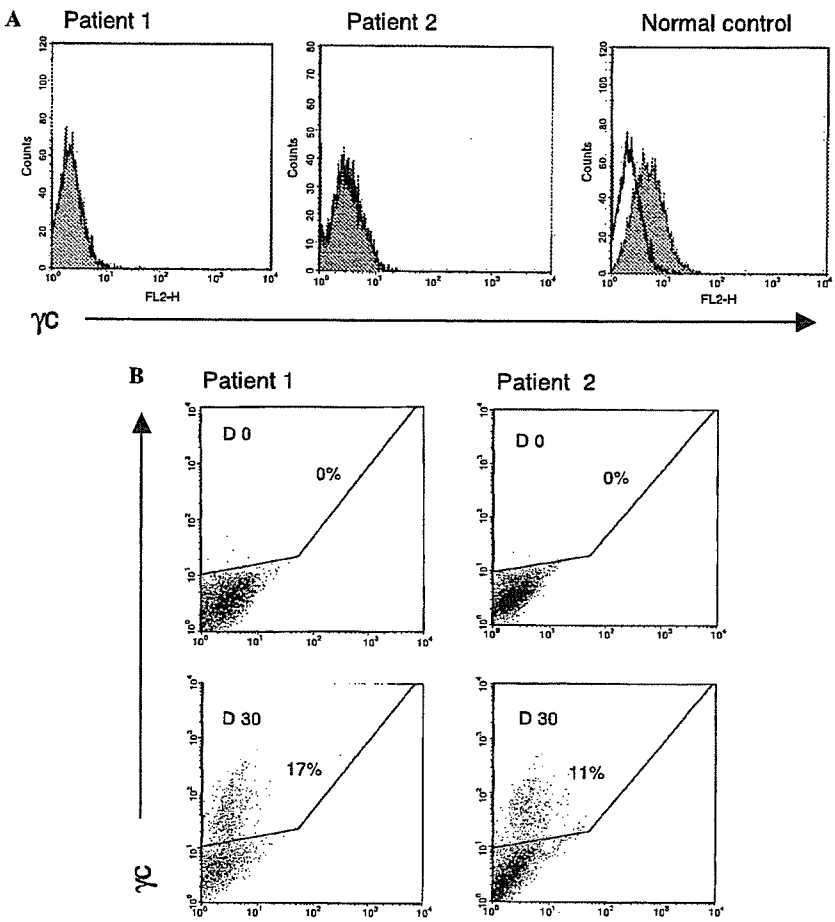

Fig. 2. Flow cytometric analysis of the γc chain expression on BCLs. (A) The γc chain expression profiles of the X-SCID BCLs and a normal control. (B) Expression of the γc chain was analyzed in transduced X-SCID BCLs immediately before (D0) and 30 days later (D30) after transduction.

Materials and methods, and Table 1. Before transduction, the γc chain was not detected on the cell surface of the X-SCID BCLs by flow cytometric analysis (Fig. 2A). One month after transduction, 17% and 11% of the X-SCID BCLs from P1 and P2 expressed the γc chain, respectively (Fig. 2B). Expression of the γc chain on the transduced BCLs was stable for more than five months (data not shown).

Functional analysis of the reconstituted γc chain

To determine whether the reconstituted γc chain could mediate intracellular signals, we examined tyrosine phosphorylation of Jak3 in response to IL-2 stimulation. Jak3 is the only tyrosine kinase known to directly associate with the γc chain and transduces signals through its phosphorylation [28,29]. Because strong constitutive tyrosine phosphorylation of Jak3 was observed in control EBV-transformed BCLs when cultured with 10% FCS, Jak3 tyrosine phosphorylation was analyzed in an optimized serum-deprived condition [30]. Under this condition, tyrosine phosphorylation of Jak3 was obvious by IL-2 stimulation in control BCLs and the γc transduced X-SCID BCLs, but not in the untransduced parental X-SCID BCLs (Fig. 3). These results demonstrated a functional reconstitution of the γc chain in X-SCID BCLs.

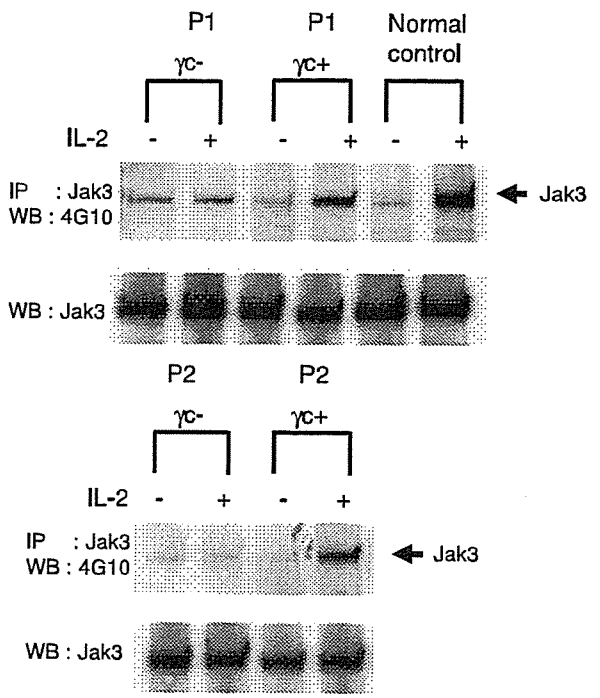

Fig. 3. Analyses of IL-2-induced Jak3 phosphorylation. The transduced and untransduced X-SCID BCLs, and a normal control were stimulated with 100 ng/ml IL-2 for 15 min, and immunoprecipitated with the Jak3 polyclonal antibody. The resultants were resolved by SDS–PAGE followed by immunoblotting with anti-phosphotyrosine antibody, 4G10.

Sensitivity of γc transduced BCLs to GCV treatment in vitro

The γc chain transduced X-SCID BCLs were cultured with various concentrations of GCV (0.1, 1.0, 10, 25, 50, and 100 μM) for 14 days. Every two days, aliquots of cells were stained with the anti-human γc chain mAb, TUGh4, to evaluate ratios of the γc chain expressing cells by flow cytometer. The γc chain positive cells were significantly decreased after 4-day culture with 10, 25, 50, and 100 μM GCV, and could not be detected within 14 days (Fig. 4A). In contrast, percentage of γc chain expressing cells in untreated BCLs was constant (data not shown). The γc expressing cells have not been detected at least for five months after cessation of GCV (Fig. 4B).

Toxicity of GCV to the non-transduced BCLs

To evaluate toxicity of GCV to the X-SCID BCLs, total cell numbers and viability were calculated each day after starting culture with various concentrations of GCV. Cell proliferation and viability of X-SCID BCLs were not affected in concentrations up to 25 μM of GCV. Whereas 50 μM GCV showed toxic effect on cell proliferation but not on cell viability. Both cell proliferation and viability were affected by 100 μM GCV (Fig. 5). Therefore, a range of GCV concentrations between 10 and 25 μM were preferable for this in vitro experiment because GCV had a suicide effect in transduced LCLs without any sign of cytotoxicity in untransduced cells.

Discussion

Retrovirus-based X-SCID gene therapy clinical trials were carried out in France and England [2,9–11]. The outcome was promising with successful immunologic reconstitution and clinical benefits in most of the patients. However, uncontrolled clonal proliferation of T cells occurred in three out of eleven patients treated in France about three years after gene therapy [12,13]. The T cell lymphoproliferation was driven by insertion of the retrovirus vector into *LMO2* locus, thereby triggering continuous and aberrant LMO-2 expression. Retroviral vectors are known to integrate into genome randomly and similar incidences of cancers due to insertional mutagenesis have been reported [16,31]. Therefore, new strategies designed to minimize the consequences of such events are needed. In this study, we have constructed a novel bicistronic vector carrying both therapeutic and suicide gene that enable selective elimination of uncontrolled proliferation of transduced lymphocytes.

The HSVtk/GCV approach has been used in several clinical trials. For example, HSVtk transduced donor T cells were infused to relapsed leukemic patient after allogeneic SCT to obtain maximum GVL effect and GCV administration. This method allows eradication of the gene modified T cells in case of GVHD [17–19]. In this trial,

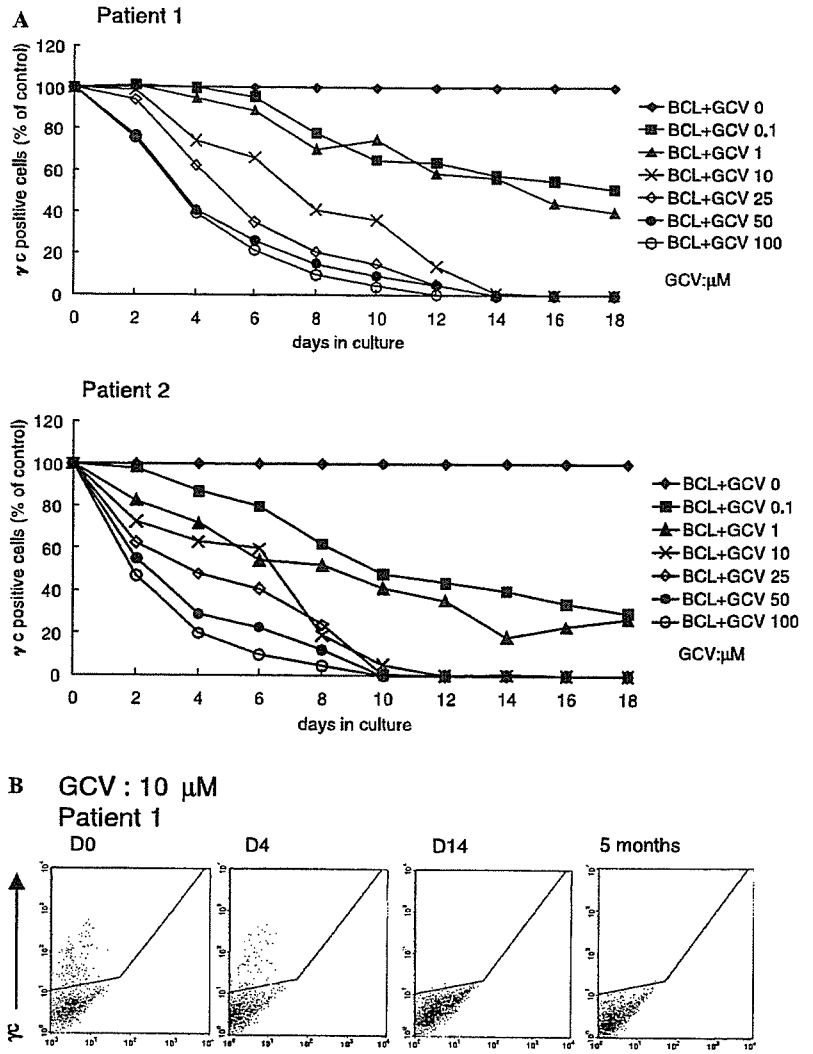

Fig. 4. Sensitivity of transduced cells to GCV treatment in vitro. (A) The γc transduced BCLs were cultured with various concentrations (0.1, 1.0, 10, 25, 50, and 100 μM) of GCV for 14 days. The transduced BCLs were grown without GCV as a control. The ratios of the γc chain expressing BCLs were expressed as relative percentages to referring control cells. (B) Representative profiles of the γc chain expression on the transduced X-SCID BCLs with 10 μM GCV.

the HSVtk transduced T cells have survived for 10 years after gene therapy and are still sensitive to GCV [32]. In this study, we applied the HSVtk/GCV system to X-SCID gene therapy as a fail-safe measure in case uncontrolled proliferation of gene transduced lymphocytes caused by insertional mutagenesis occurred. After transduction of X-SCID BCLs with the retrovirus vector carrying the γc chain and HSVtk genes, the transduced cells were treated with various concentrations of GCV in vitro. All transduced cells were eliminated at 10 μM GCV for 14 days. Concentrations of GCV required for elimination of HSVtk transduced cells were reported to vary among different cell lines [33]. Bonnekoh et al. [34] reported that 40 μM GCV is necessary to eliminate all the HSVtk transduced melanoma cells, whereas Verzeletti et al. [18] showed that HSVtk transduced lymphocytes were sensitive and completely eliminated at 1 μM GCV in vitro. Based on the studies mentioned above, the concentration of GCV is dependent upon the nature of cell line used. Therefore, we speculated that relatively higher concentration of GCV (10 μM) is required in this experiment due to the relatively higher GCV resistance of patients' B-cell lines compared with normal lymphocytes.

It is also important to evaluate cytotoxicity of GCV because it has severe side effects such as myelosuppression, immunosuppression, and renal failure. Crumpacker [35] reported pharmacokinetic analysis of intravenous administration of GCV. A typical clinical use (10 mg of GCV per kilogram per day in two divided doses) results in a peak serum concentration of 40 μM and a trough concentration of 3 μM. We have determined a range of GCV that can eliminate transduced BCLs without causing cytotoxicity in vitro. The determined range of GCV in our study was within the peak and trough level. If target cells were clon-

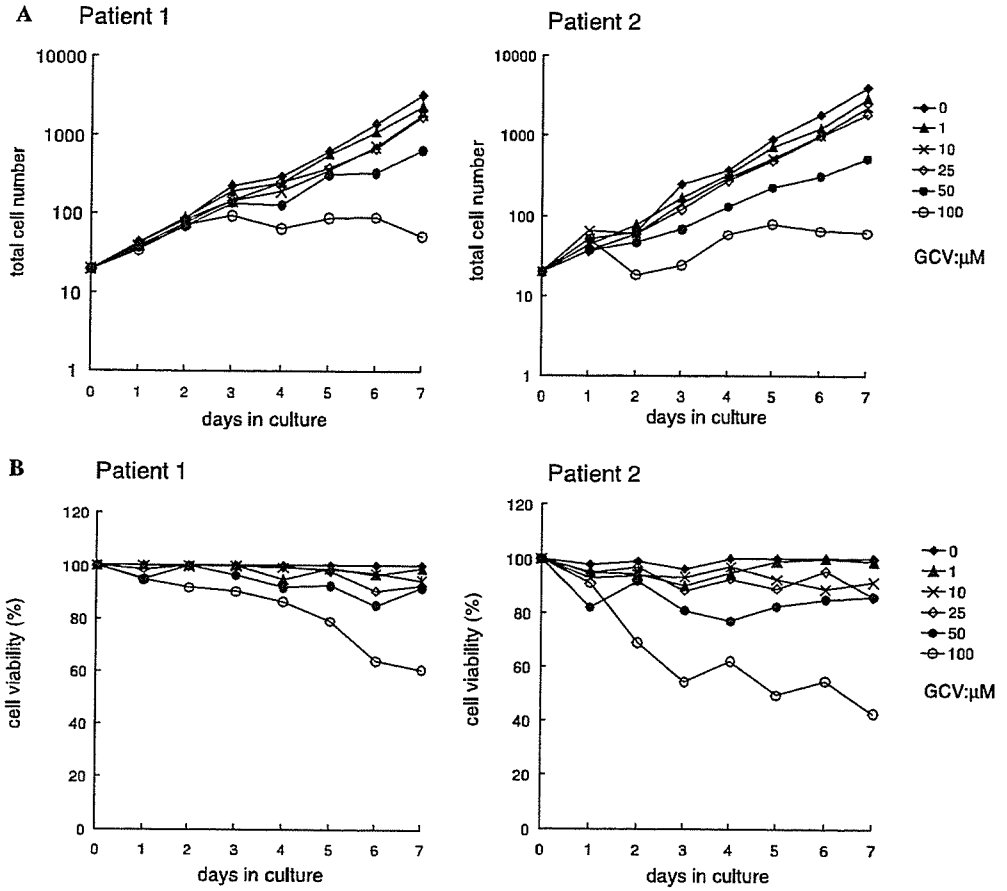

Fig. 5. Cell proliferation and viability. Cytotoxicity of GCV was evaluated by cell proliferation and viability in non-transduced BCLs. Cell proliferation and viability were calculated every day for 7 days. (A) Proliferation was estimated by plotting of total number of cells each day. (B) The percentage of viable cells was calculated by trypan blue exclusion.

ally expanded T lymphocytes due to retroviral insertion mutagenesis, lower concentrations of GCV would be effective because previous report demonstrated that HSVtk transduced lymphocytes were completely eliminated at 1 μM of GCV in vitro [18].

Escape mechanisms of suicide gene such as chromosomal deletion and silencing of HSVtk gene can influence the outcome of GCV treatment [36]. Silencing of HSVtk gene is a serious problem because it results in continuous cell proliferation even after GCV treatment. To overcome gene silencing, the MSCV LTR-based vector used in this experiment is engineered to resist de novo methylation [37–39]. The LTR differs from the MoMLV LTR by nine point mutations and deletion of one of the 75-bp repeats in the U3 region [37]. These changes enhance transcriptional activation and prevent transcriptional suppression. In addition, to ensure the co-expression of the γc chain and HSVtk genes, IRES element was employed in the bicistronic retroviral vector because it permits translation of two genes simultaneously from a single transcriptional unit. With the modified MSCV LTR-based bicistronic vector, pD-γc/TK, the transduced X-SCID BCLs expressed the γc chain stably and remained sensitive to GCV for more than five months.

Host immune response might be generated against the HSVtk suicide gene, leading to elimination of the transduced cells [18]. However, the possibility that HSVtk would induce immune reaction after gene therapy is less likely due to profound impairment of cellular and humoral immunity in X-SCID patients. Furthermore, HSVtk is recognized as a self-antigen because T cell progenitor cells had already expressed the gene prior to thymus migration.

One might argue that all stem cells carrying the γc chain gene will be eliminated with the HSVtk/GCV approach. However, we hypothesized that a small proportion of resting hematopoietic stem cells can escape from GCV treatment because only proliferating cells are sensitive to GCV. The escaped hematopoietic stem cells would reconstitute the immune system, whereas the actively proliferating cells caused by insertional mutagenesis are killed after GCV treatment.

The result of the present study using a novel therapeutic bicistronic retrovirus vector carrying both causative and suicide gene is encouraging. Currently, we are testing the efficacy and safety feature of this bicistronic retroviral vector in an X-SCID murine model.

Acknowledgments

The authors are thankful to Ms. Ikuko Hakozaki and Mr. Looi Chung Yeng for their help with sequencing analysis of the X-SCID patients and with English correction of the manuscript, respectively. This study was financially supported by Grants-in-Aid for Scientific Research from Japan Society for the Promotion of Science, and a grant from the Ministry of Health, Labor and Welfare, Japan.

References

[1] M. Noguchi, H. Yi, H.M. Rosenblatt, A.H. Filipovich, S. Adelstein, W.S. Modi, O.W. Mcbride, W.J. Leonard, Interleukin-2 receptor gamma chain mutation results in X-linked severe combined immunodeficiency in humans, Cell 73 (1993) 147–157.

[2] A. Fischer, F. Le Deist, S. Hacein-Bey-Abina, I. Andre-Schmutz, G. de Saint Basile, J.P. de Villartay, M. Cavazzana-Calvo, Severe combined immunodeficiency. A model disease for molecular immunology and therapy, Immunol. Rev. 203 (2005) 98–109.

[3] K. Sugamura, H. Asao, M. Kondo, N. Tanaka, N. Ishii, K. Ohbo, M. Nakamura, T. Takeshita, The interleukin-2 receptor γ chain: its role in the multiple cytokine receptor complexes and T cell development in XSCID, Annu. Rev. Immunol. 14 (1996) 179–205.

[4] T. Takeshita, H. Asao, K. Ohtani, N. Ishii, S. Kumaki, N. Tanaka, H. Munakata, M. Nakamura, K. Sugamura, Cloning of the γ chain of the human IL-2 receptor, Science 257 (1992) 379–382.

[5] H. Asao, C. Okuyama, S. Kumaki, N. Ishii, S. Tsuchiya, D. Foster, K. Sugamura, Cutting edge: the common γ-chain is an indispensable subunit of the IL-21 receptor complex, J. Immunol. 167 (2001) 1–5.

[6] C. Antoine, S. Muller, A. Cant, M. Cavazzana-Calvo, P. Veys, J. Vossen, A. Fasth, C. Heilmann, N. Wulffraat, R. Seger, S. Blanche, W. Friedrich, M. Abinun, G. Davies, R. Bredius, A. Shulz, P. Landais, A. Fischer, Long-term survival and transplantation of hematopoietic stem cells for immunodeficiencies: report of the European experience 1968–1999, Lancet 361 (2003) 553–560.

[7] R.H. Buckley, S.E. Schiff, R.I. Schiff, L. Markert, L.W. Williams, J.L. Roberts, L.A. Myers, F.E. Ward, Hematopoietic stem-cell transplantation for the treatment of severe combined immunodeficiency, N. Engl. J. Med. 340 (1999) 508–516.

[8] E. Haddad, P. Landais, W. Friedrich, B. Gerritsen, M. Cavazzana-Calvo, G. Morgan, Y. Bertrand, A. Fasth, F. Porta, A. Cant, T. Espanol, S. Muller, P. Veys, J. Vossen, A. Fischer, Long-term immune reconstitution and outcome after HLA-nonidentical T-cell-depleted bone marrow transplantation for severe combined immunodeficiency: a European retrospective study of 116 patients, Blood 91 (1998) 3646–3653.

[9] M. Cavazzana-Calvo, S. Hacein-Bey, G. de Saint Basile, F. Gross, E. Yvon, P. Nusbaum, F. Selz, C. Hue, S. Certain, J.L. Casanova, P. Bousso, F.L. Deist, A. Fischer, Gene therapy of human severe combined immunodeficiency (SCID)-X1 disease, Science 288 (2000) 669–672.

[10] S. Hacein-Bey-Abina, A. Fischer, M. Cavazzana-Calvo, Gene therapy of X-linked severe combined immunodeficiency, Int. J. Hematol. 76 (2002) 295–298.

[11] H.B. Gaspar, K.L. Parsley, S. Howe, D. King, K.C. Gilmour, J. Sinclair, G. Brouns, M. Schmidt, C. Von Kalle, T. Barington, M.A. Jakobsen, H.O. Christensen, A. Al Ghonaium, H.N. White, J.L. Smith, R.J. Levinsky, R.R. Ali, C. Kinnon, A.J. Thrasher, Gene therapy of X-linked severe combined immunodeficiency by use of a pseudotyped gammaretroviral vector, Lancet 364 (2004) 2181–2187.

[12] S. Hacein-Bey-Abina, C. Von Kalle, M. Schmidt, M.P. McCormack, N. Wulffraat, P. Leboulch, A. Lim, C.S. Osborne, R. Pawliuk, E. Morillon, R. Sorensen, A. Forster, P. Fraser, J.I. Cohen, G. de Saint Basile, I. Alexander, U. Wintergerst, T. Frebourg, A. Aurias, D. Stoppa-Lyonnet, S. Romana, I. Radford-Weiss, F. Gross, F. Valensi, E. Delabesse, E. Macintyre, F. Sigaux, J. Soulier, L.E. Leiva, M. Wissler, C. Prinz, T.H. Rabbitts, F. Le Deist, A. Fischer, M. Cavazzana-Calvo, LMO2-associated clonal T cell proliferation in two patients after gene therapy for SCID-X1, Science 302 (2003) 415–419.

[13] E. Check, Gene therapy put on hold as third child develops cancer, Nature 433 (2005) 561.

[14] A.A. Ferrando, S. Herblot, T. Palomero, M. Hansen, T. Hoang, E.A. Fox, A.T. Look, Biallelic transcriptional activation of oncogenic transcription factors in T-cell acute lymphoblastic leukemia, Blood 103 (2004) 1909–1911.

[15] U.P. Dave, N.A. Jenkins, N.G. Copeland, Gene therapy insertional mutagenesis insights, Science 303 (2004) 333.

[16] R. Seggewiss, S. Pittaliga, R. Adler, C. Ferguson, E.F. Vanin, P.F. Kelly, R.E. Donahue, B.P. Sorrentiono, A.W. Nienhuis, C.E. Dunbar, Myeloid sarcoma associated with gene marking of hematopoietic stem cells in a rhesus macaque, Mol. Ther. 11 (Suppl. 1) (2005) S150.

[17] C. Bonini, G. Ferrari, S. Verzeletti, P. Servida, E. Zappone, L. Ruggieri, M. Ponzoni, S. Rossini, F. Mavilio, C. Traversari, C. Bordignon, HSV-TK gene transfer into donor lymphocytes for control of Allogenic Graft-versus-leukemia, Science 276 (1997) 1719–1724.

[18] S. Verzeletti, C. Bonini, S. Marktel, N. Nobili, F. Ciceri, C. Traversari, C. Bordignon, Herpes simplex virus thymidine kinase gene transfer for controlled graft-versus-host disease and graft-versus-leukemia: clinical follow-up and improved new vectors, Hum. Gene Ther. 9 (1998) 2243–2251.

[19] A. Bondanza, F. Ciceri, C. Bonini, Application of donor lymphocytes expressing a suicide gene for early GVL induction and later control of GVH reactions after bone-marrow-transplantation, Methods Mol. Med. 109 (2005) 475–486.

[20] Z. Ram, K.W. Culver, E.M. Oshiro, J.J. Viola, H.L. De Vroom, E. Otto, Z. Long, Y. Chiang, G.J. McGarrity, L.M. Muul, D. Katz, R.M. Blaese, E.H. Oldfield, Therapy of malignant brain tumors by intratumoral implantation of retroviral vector-producing cells, Nat. Med. 3 (1997) 1354–1361.

[21] D. Klatzmann, P. Cherin, G. Bensimon, O. Boyer, A. Coutellier, F. Charlotte, C. Boccaccio, J.L. Salzmann, S. Herson, A phase I/II dose-escalation study of herpes simplex virus type I thymidine kinase "suicide" gene therapy for metastatic melanoma, Hum. Gene Ther. 9 (1998) 2585–2594.

[22] N.G. Rainov, A phase III clinical evaluation of herpes simplex virus type I thymidine kinase and ganciclovir gene therapy as an adjuvant to surgical resection and radiation in adults with previously untreated globlastoma multiforme, Hum. Gene Ther. 11 (2000) 2389–2401.

[23] J.L. Roberts, D.J. Volkman, R.H. Buckley, Modified MHC restriction of donor-origin T cells in humans with severe combined immunodeficiency transplanted with haploidentical bone marrow stem cells, J. Immunol. 143 (1989) 1575–1579.

[24] S. Kumaki, N. Ishii, M. Minegishi, Y. Ohashi, I. Hakozaki, S. Nonoyama, K. Imai, T. Morio, I. Tsuge, Y. Sakiyama, A. Miyanoshita, J. Miura, M. Mayumi, T. Heike, K. Katamura, H. Takada, I. Izumi, J. Kamizono, S. Hibi, H. Sasaki, M. Kimura, A. Kikuta, Y. Date, M. Sako, H. Tanaka, K. Sano, K. Sugamura, S. Tsuchiya, Characterization of the γc chain among 27 unrelated Japanese patients with X-linked severe combined immunodeficiency (X-SCID), Hum. Genet. 107 (2000) 406–408.

[25] N. Ishii, H. Asao, Y. Kimura, T. Takeshita, M. Nakamura, S. Tsuchiya, T. Konno, M. Maeda, T. Uchiyama, K. Sugamura, Impairment of ligand binding and growth signaling of mutant IL-2 receptor γ-chains in patients with X-linked severe combined immunodeficiency, J. Immunol. 153 (1994) 1310–1317.

[26] J.C. Burns, T. Friedmann, W. Driever, M. Burrascano, J.K. Yee, Vesicular stomatitis virus G glycoprotein pseudotyped retroviral vectors: concentration to very high titer and efficient gene transfer into mammalian and nonmammalian cells, Proc. Natl. Acad. Sci. USA 90 (1993) 8033–8037.

[27] A.D. Miller, J.V. Garcia, N. von Suhr, C.M. Lynch, C. Wilson, M.V. Eiden, Construction and properties of retrovirus packaging cells based on gibbon ape leukemia virus, J. Virol. 65 (1991) 2220–2224.
[28] S.M. Russell, J.A. Jhonston, M. Noguchi, M. Kawamura, C.M. Bacon, M. Friedmann, M. Berg, D.W. McVicar, B.A. Witthuhn, O. Silvennoinen, Interaction of IL-2R β and the γ chain with Jak1 and Jak3: implications for XSCID and XCID, Science 266 (1994) 1042–1045.
[29] T. Miyazaki, A. Kawahara, H. Fujii, Y. Nakagawa, Y. Minami, Z.J. Liu, I. Oishi, O. Silvennoinen, B.A. Witthuhn, J.N. Ihle, Functional activation of Jak1 and Jak3 by selective association with IL-2 receptor subunits, Science 266 (1994) 1045–1047.
[30] H. Hacein-Bey, M. Cavazzana-Calvo, F. Le Deist, A. Dautry-Varsat, C. Hivroz, I. Riviere, O. Danos, J.M. Heard, K. Sugamura, A. Fischer, G. De Saint Basile, γc gene transfer into SCID X1 patients' B-cell lines restores nomal high-affinity interleukin-2 receptor expression and function, Blood 87 (1996) 3108–3116.
[31] U. Modlich, O.S. Kustikova, M. Schmidt, C. Rudolph, J. Meyer, Z. Li, K. Kamino, N. von Neuhoff, B. Schlegelberger, K. Kuehlcke, K.D. Bunting, S. Schmidt, A. Deichmann, C. von Kalle, B. Fehse, C. Baum, Leukemias following retroviral transfer of multidrug resistance 1 (MDR1) are driven by combinational insertional mutagenesis, Blood 105 (2005) 4235–4246.
[32] A. Recchia, Z. Magnani, F. Urbinati, D. Sartori, S. Muraro, M.T. Lupo Stanghellini, M. Bernardi, A. Pescarollo, M. Bregni, C. Bonini, C. Bordignon, F. Ciceri, F. Mavilio, Molecular follow-up of patient treated with allogeneic hematopoietic stem cell transplantation and donor lymphocytes transduced with a retroviral vector expressing HSV-TK and ΔLNGFR [abstract], Mol. Ther. 11 (Suppl 1) (2005) S318.
[33] C. Beck, S. Cayeux, S.D. Lupton, B. Dorken, T. Blankenstein, The thymidine kinase/ganciclovir-mediated "suicide" effect is variable in different tumor cells, Hum. Gene Ther. 6 (1995) 1525–1530.
[34] B. Bonnekoh, D.A. Greenhalgh, D.S. Bundman, J.N. Eckhardt, M.A. Longley, S.H. Chen, S.L. Woo, D.R. Roop, Inhibition of melanoma growth by adenoviral-mediated HSV thymidine kinase gene transfer in vivo, J. Invest. Dermatol. 104 (1995) 313–317.
[35] C.S. Crumpacker, Drug therapy; Ganciclovir, N. Engl. J. Med. 335 (1996) 721–729.
[36] O. Frank, C. Rudolph, C. Heberlein, N. von Neuhoff, E. Schrock, A. Schambach, B. Schlegelberger, B. Fehse, W. Ostertag, C. Stocking, C. Baum, Tumor cells escape suicide gene therapy by genetic and epigenetic instability, Blood 104 (2004) 3543–3549.
[37] R.G. Hawley, F.H. Lieu, A.Z. Fong, T.S. Hawley, Versatile retroviral vectors for potential use in gene therapy, Gene Ther. 1 (1994) 136–138.
[38] A. Suzuki, K. Obi, T. Urabe, H. Hayakawa, M. Yamada, S. Kaneko, M. Onodera, Y. Mizuno, H. Mochizuki, Feasibility of ex vivo gene therapy for neurological disorders using the new retroviral vector GCDNsap packaged in the vesicular stomatitis virus G protein, J. Neurochem. 82 (2002) 953–960.
[39] S. Kaneko, T. Nagasawa, H. Nakauchi, M. Onodera, An in vivo assay for retrovirally transduced human peripheral T lymphocytes using nonobese diabetic/severe combined immunodeficiency mice, Exp. Hematol. 33 (2005) 35–41.

Available online at www.sciencedirect.com
SCIENCE DIRECT®
Virology 349 (2006) 254–263
VIROLOGY
www.elsevier.com/locate/yviro

Rapid Communication

Survival of parvovirus B19-infected cells by cellular autophagy

Akitoshi Nakashima [a,d], Nobuyuki Tanaka [a,*], Keiichi Tamai [a], Masanao Kyuuma [a], Yoshinori Ishikawa [a], Hiroyuki Sato [b], Tamotsu Yoshimori [c], Shigeru Saito [d], Kazuo Sugamura [a]

[a] *Department of Microbiology and Immunology, Tohoku University Graduate School of Medicine, 2-1 Seiryo-machi, Aoba-ku, Sendai 980-8575, Japan*
[b] *Fukuoka Red Cross Blood Center, Fukuoka 818-8588, Japan*
[c] *Department of Cell Genetics, National Institute of Genetics, Mishima 411-8540, Japan*
[d] *Department of Obstetrics and Gynecology, Toyama Medical and Pharmaceutical University School of Medicine, 2630 Sugitani, Toyama 930-0194, Japan*

Received 30 November 2005; returned to author for revision 26 January 2006; accepted 21 March 2006
Available online 27 April 2006

Abstract

Human parvovirus B19 (B19) is a well-known pathogenic agent which causes apoptosis in erythrocyte lineage cells. Here, we provide the first evidence that mitochondrial autophagy is specifically found in the B19-infected cells. The protein expression ratio for LC3-II/LC3-I increased significantly in infected cells, indicating possible involvement of cellular autophagy in the infection process. Immunofluorescence confocal microscopy analyses revealed that B19 infection induced an intracellular autophagosome as judged by endogenous LC3 staining. Moreover, inhibition of autophagy by 3-MA significantly facilitated B19-infection-mediated cell death. These results suggest a novel mechanism by which B19-infected cells survive by cellular autophagy.

Keywords: Parvovirus B19; Autophagy; LC3; 3-MA

Introduction

Cellular homeostasis is controlled by a balance of protein biosynthesis and degradation. Eukaryotic cells utilize at least two distinct pathways to degrade intracellular proteins, namely ubiquitin/proteasome- and lysosome-dependent degradation. Accumulating evidences suggest that most short-lived proteins are tagged with polyubiquitin chains and destined to be degraded by proteasomes, whereas those with relatively longer half-lives are sorted into intracellular vesicles called endosomes and lysosomes, allowing them to be digested by acid proteases. Upon exposure to various cellular stresses, including nutrient starvation and bacterial infection, the third cellular degradation system is activated that sequestrates a part of cytoplasm, organella, and pathogens. This bulk degradation system, called autophagy, is characterized as a process by which a portion of a cytoplasm including organelle gets surrounded by a so-called "isolation membrane". A small portion of cytoplasm enclosed by the de novo synthesized autophagic isolation membrane falls within the double-membrane structure, called autophagosomes. Then the vacuole membrane fuses with the lysosome, where the cytoplasm-derived materials are degraded and/or recycled.

Accumulating evidences suggest biological significance of autophagy. Although a basal level of autophagy may be routinely used to clear away intracellular proteins and organellas and is required for normal turnover of cellular components, activation of autophagy is also associated with physiological response to environmental stress. Upon nutrient starvation, for example, autophagy is required for cell survival in yeast as well as in mammals (Yoshimori, 2004). Paradoxically, upon various stresses, autophagy also plays crucial roles in programmed cell death (PCD). A caspase-independent cell death called 'Type II' programmed cell death (PCD) is characterized by an accumulation of autophagic vesicles. Further, a recent study showed that inhibition of caspase activity induces autophagy in certain cells (Yu et al., 2004), suggesting that both type I and type II PCDs may utilize autophagy. Pathogen infection is another typical 'life-threatening' stress on cells. Streptococcus pyogenes,

* Corresponding author. Fax: +81 22 717 8097.
E-mail address: n-tanaka@mail.tains.tohoku.ac.jp (N. Tanaka).

0042-6822/$ - see front matter © 2006 Elsevier Inc. All rights reserved.
doi:10.1016/j.virol.2006.03.029

known as Group A streptococcus (GAS) that invades non-phagocytic cells to escape into the cytoplasm, is eventually captured and sequestrated by autophagosomes (Nakagawa et al., 2004). In the context of intracellular pathogens, a close relationship between autophagy and some viral infection has been documented, including a double-stranded DNA virus such as herpes simplex virus 1 (HSV1) and single-stranded RNA virus species including murine hepatitis virus (MHV) and poliovirus (PV). Although autophagy is inhibited by a viral protein in HSV, it is conversely utilized for the viral replication in MHV and PV infection (Kirkegaard et al., 2004). Thus, the role of autophagy in the host seems to be dependent on each specific viral strain, but the overall relevance is still controversial.

Human parvovirus B19 is one of the smallest single-stranded DNA virus, which lacks an envelope and infects erythroid (progenitor) cells to cause several diseases including aplastic crisis in patients with hemolytic anemia, erythema infectiosum and hydrops fetalis. We and others have documented that B19 infection induces cell cycle arrest at G1 and G2/M phases, and apoptosis mediated by NS1, a non-structural protein encoded by the viral genome (Kirisako et al., 2000; Morita and Sugamura, 2002; Morita et al., 2001, 2003; Nakashima et al., 2004). Thus, apoptosis has been well documented regarding the B19-infected cells. Moreover, we have repeatedly found the enlargement of the infected cells, without a known biological significance. Here, we provide the first evidence that cellular autophagy is specifically found in the B19-infected enlarged cells and is involved in the survival of these cells.

Results

Infection of B19 parvovirus induces an FSC^{high} SSC^{high} cell population

Accumulating evidences suggest that B19 parvovirus shows cytotoxic activity against host cells including erythroid precursors (Ozawa et al., 1987; Young et al., 1984). In order to examine if the infection of B19 parvovirus induces any morphological changes on affected cells, we transduced the virus onto B19-susceptible erythroid cell line, UT7/Epo-S1. In our preliminary experiments, a morphologically distinct cell population characterized by the enlargement in cell size was observed at 48 h after the B19 virus infection (Morita et al., 2001). To further characterize the cell population, we utilized FACS analyses. When compared with mock-infected cells, a newly emerging high forward scatter (FSC) and high side scatter (SSC) cell population ($FSC^{high}SSC^{high}$; hereafter referred as population "B19-B"), was clearly visible in the B19-infected cell population (Fig. 1A). The percentages of B19-B in cell number were 34.8% and 1.8% for B19- and mock-infected cells, respectively. To determine whether the population B19-B is indeed induced by the viral infection, we checked NS1 protein expression, which is a hallmark of B19 infection. After sorting the B19-infected cells into the two distinct populations, $FSC^{med}SSC^{low}$ (hereafter referred as population "B19-A") and B19-B, cells from each population were stained with an anti-NS1 antibody. The percentages of NS1-positive cells were 28.8% and 84.6% in population of B19-A and B19-B, respectively (Fig. 1B). Since the NS1-positive cell number observed in B19-B population was significantly higher than that of the B19-A, we conclude that the B19-B population is most likely induced by the B19 infection.

Since our former study indicated that growth arrest of cells at G2 phase is highly associated with B19 infection, we examined both B19-A and B19-B populations for their cell cycle status. In the B19-infected B19-B population, cells within G2/M were 78%, as compared to 25% in B19-A, and 15% in mock-infected B19-A populations (Fig. 1C). Consistent with the clear difference observed among the three cell populations examined, cells from the B19-infected B19-B population grew significantly slower than those from the B19-A populations from B19-infected or uninfected cells (Fig. 1D). Additionally, appearance of the B19-B population was completely abrogated by the pretreatment of B19 virus with anti-B19 virus neutralizing antibody-positive, but not -negative human serum (data not shown). Collectively, these results indicate that B19 infection induced the unique B19-B population characterized by the "G2-arrested" phenotype.

B19 infection induces autophagosome-like vesicles

To further characterize the B19-B population, we next examined the permeability of mitochondria and plasma membranes in B19-infected cells, because we suspect that the FSC^{high} phenotype indicates the enlargement of cell size which is an outcome of the increase in cell membrane permeability. However, no significant difference was detected, suggesting that neither oncosis nor typical apoptosis mediates the B19-induced changes (data not shown). Because the high SSC in FACS analyses is likely to represent the higher 'complexity' within the cytoplasm, we then decided to directly examine the intracellular organization of cells from the B19-B population by electron microscopy (EM). On days 2 and 5 after the B19 infection, cells were fixed and subjected to the analyses. A remarkable difference in cell morphology was observed; most of the B19-infected cells were relatively larger with diameter of approximately 16–24 μm, whereas that of mock-transfected cells were only 8–9 μm (Figs. 2Aa, b, and c). The percentages of cells having diameters of more than 15 μm were $2.6 \pm 1.2\%$, $48.7 \pm 3.7\%$ and $11.6 \pm 3.0\%$ in mock-infected, day two and day five of the B19 infection, respectively (Fig. 2B). Another significant difference observed in the infected cells on day 2 was the shape of their nuclei, which manifested lower EM density with swollen shape and ruffled nuclear membranes. In addition to the altered morphology of the nuclei, the size of the cytoplasm was quite enlarged. Of note, many EM-dense spherical structures were scattered among the cytoplasm. These membrane surrounded structures were observed more frequently in the larger sized than the normal-sized cells on day 2 after the infection (Fig. 2Ah). Some of the membrane surrounded structures seemed to contain degraded mitochondria with double membrane structure (Figs. 2Ah and k). Taking into account the 'vesicles' with double-membrane like

structure, we speculated that these organellas most resemble autophagosomes. Interestingly, the autophagosome like vesicles showed increase in their size from an average diameter of 0.2 μm to 0.6 μm on day 5 (Figs. 2Ai and l). Unlike the B19 infection, mock infection did not induce any of these changes (Figs. 2Ag and j). Furthermore, a significant percentage of

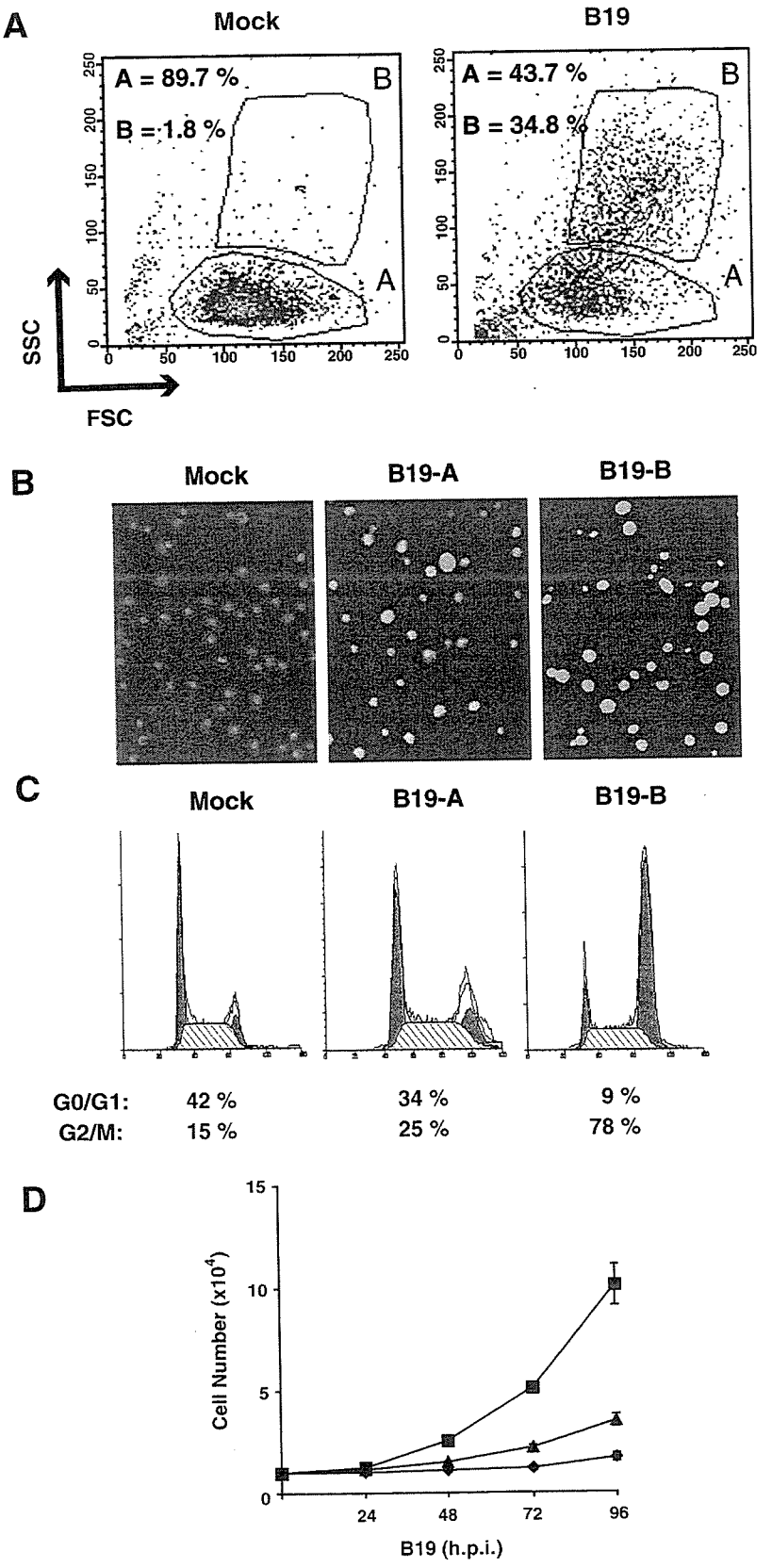

cells manifested shrunk morphology and higher EM density (Figs. 2Ac, arrows), suggesting an increase in cells with apoptotic phenotype on day 5 compared with negligible number of cells with similar phenotype on day 2 or mock-infected cells (Figs. 2Aa, b, and c). Therefore, both apoptotic and autophagic cells were detected on day 5 (Fig. 2Ai). Taken together, these results suggest that B19 infection induced not only smaller apoptotic cells but also enlarged cells carrying significant numbers of autophagosome-like vesicles.

Activation of autophagy in B19-infected cells

To further examine whether the autophagosome like vesicles frequently found within the B19-infected cells indeed represent activation of autophagy in these cells, we tested the expression of LC3, which specifically labels autophagosome and thus is a hallmark of autophagy. At quiescent status, LC-3 basically resides in the cytoplasm as a precursor form, LC3-I. However, upon exposure to various environmental stresses to provoke autophagy, it is rapidly degraded to produce a lipidated form, LC3-II, which then sticks onto autophagosomes. Therefore, the LC3-II/LC3-I ratio well correlates with the number of autophagosomes (Kabeya et al., 2000). We infected UT7/Epo-S1 cells with B19. Cell lysates prepared from cells at 96 h post-infection were subjected to Western blot analysis. We found time-dependent increase of the LC3-II/LC3-I ratio, which maximized at 96 h post-infection (Figs. 3A and B). Accordingly, expression of NS1 also maximized at the same 96 h post-infection (Fig. 3A).

To further clarify whether autophagy occurs in B19-infected cells, we next immunostained endogenous LC3 on fixed cells and analyzed by the immunofluorescence confocal microscopy. In the mock-transfected cells, LC3 was diffusely expressed under a non-starved condition (Fig. 3C). Upon B19 infection, however, LC3-positive larger dots that represent autophagosomes, were clearly identified mostly within the cytoplasm as judged by the simultaneous staining of NS1 protein, which resides within the nucleus. Noteworthy, LC3-positive autophagosomes were only detected in NS1-positive cells, but not in NS1-negative cells (Fig. 3C). These results indicate that B19-induces autophagy that maximizes at 96 h post-infection, with good accordance with NS1-expression.

B19-induced autophagy correlates with survival of infected cells

We next explored a biological significance of autophagy in B19-infected cells. To clarify whether abrogation of autophagosome formation has any effect on infected cells, we performed B19 infection experiments using UT7/Epo-S1 cells in the presence or absence of a specific autophagy inhibitor, 3-methyladenine (3-MA). At 48 h after the infection, 3-MA was added to the culture and further incubated for additional 24 h. To examine whether blockade of autophagy may alter the cell viability, cells in the sub-G1 fraction, which represent dead cells, were analyzed by a flow cytometry. Surprisingly, percentage of dead cells after the B19 infection showed significant increase in the presence of 3-MA; 27% and 12%, in the presence or absence of 3-MA, respectively (Fig. 4A). This increase in dead cells by the abrogation of autophagy is rather specific to B19 infection because mock-transfected cells conferred little if any alteration in the viability. On the other hand, 3-MA did not alter the NS1 expression, irrespective of B19 infection as judged by the immunocytochemical analyses suggesting similar B19 infection efficiency (data not shown). To further clarify the effect of autophagy inhibitor on B19-induced cell death, we determined to quantify the 'Autophagic Cell Death Index' (hereafter referred as ACD index), which is calculated by the ratio of dead cells in the presence and absence of 3-MA (3-MA(+)/3-MA(−)). This index is expected to represent effects of autophagy inhibitor on B19- or mock-infected cells. After the initial B19 infection period of 24, 48, 72, and 96 h, cells were cultured in the presence or absence of the 3-MA for additional 24 h, and the numbers of dead cells were determined. For a control, cells without infection (referred as "0 h" infection) were incubated in the presence or absence of 3-MA for 24 h. The ACD index on B19 infection showed 1.7-fold increase at 24 h after the infection, which maximized up to 2.5 at 48 h, whereas little if any effects of 3-MA on mock-infected cells (Fig. 4B). Finally, we examined the ACD index in a time-dependent manner by 3-MA treatment on cells at 48 h time point after the B19 infection (Fig. 4C). When B19-infected cells were used for this assay, the ACD index showed a modest increase at the initial 12-h time point after the 3-MA incubation and a maximum score was obtained at 24 h after the treatment. On the other hand, almost negligible increase was observed in the mock infection, suggesting little if any effect of 3-MA on cell death. Collectively, these results suggest that autophagy is involved in the survival of B19-infected cells which is most prominent at later stages of infection including 48 to 96 h after infection.

Discussion

In the present study, we provide the first evidence that cellular autophagy is induced by the human parvovirus B19. Autophagy induced in the B19-susceptible UT7/Epo-S1 cells is at least partially required for the infected cell survival.

In this study, we identified a novel cell population, B19-B, after B19 infection (Figs. 1A, B). This new population, because

Fig. 1. (A) Identification of a unique population in B19-infected cells (Upper panels). Flow cytometric analyses of UT7/Epo-S1 cells which were infected with B19 virus for 48 h. Cells were infected with B19 virus (right) and mock (left). The percentages of cell numbers in area A ($FSC^{high}SSC^{low}$) and B ($FSC^{high}SSC^{high}$) are shown. (B) Expression of NS1 in B19-infected cells. B19-infected cells were immunolabeled with anti-NS1 and FITC-conjugated anti-mouse IgG secondary antibody (green). Nuclei were detected by DNA staining with 4′,6′-diamidino-2-phenylindole (blue). (C) Cell cycle analysis of B19-infected populations. After segmentation, B19-infected or mock-infected cells were labelled with PI to detect DNA content and analyzed by FACS caliber. (D) Cell growth of B19 virus-infected-A, B and mock-infected UT7/Epo-S1 cells. UT7/Epo-S1 cells were infected with B19 virus and counted. Area A (triangles), area B (diamonds) of B19 infection or mock infection (squares) are indicated. Experimental data presented are representative of at least three experimental data with similar results.

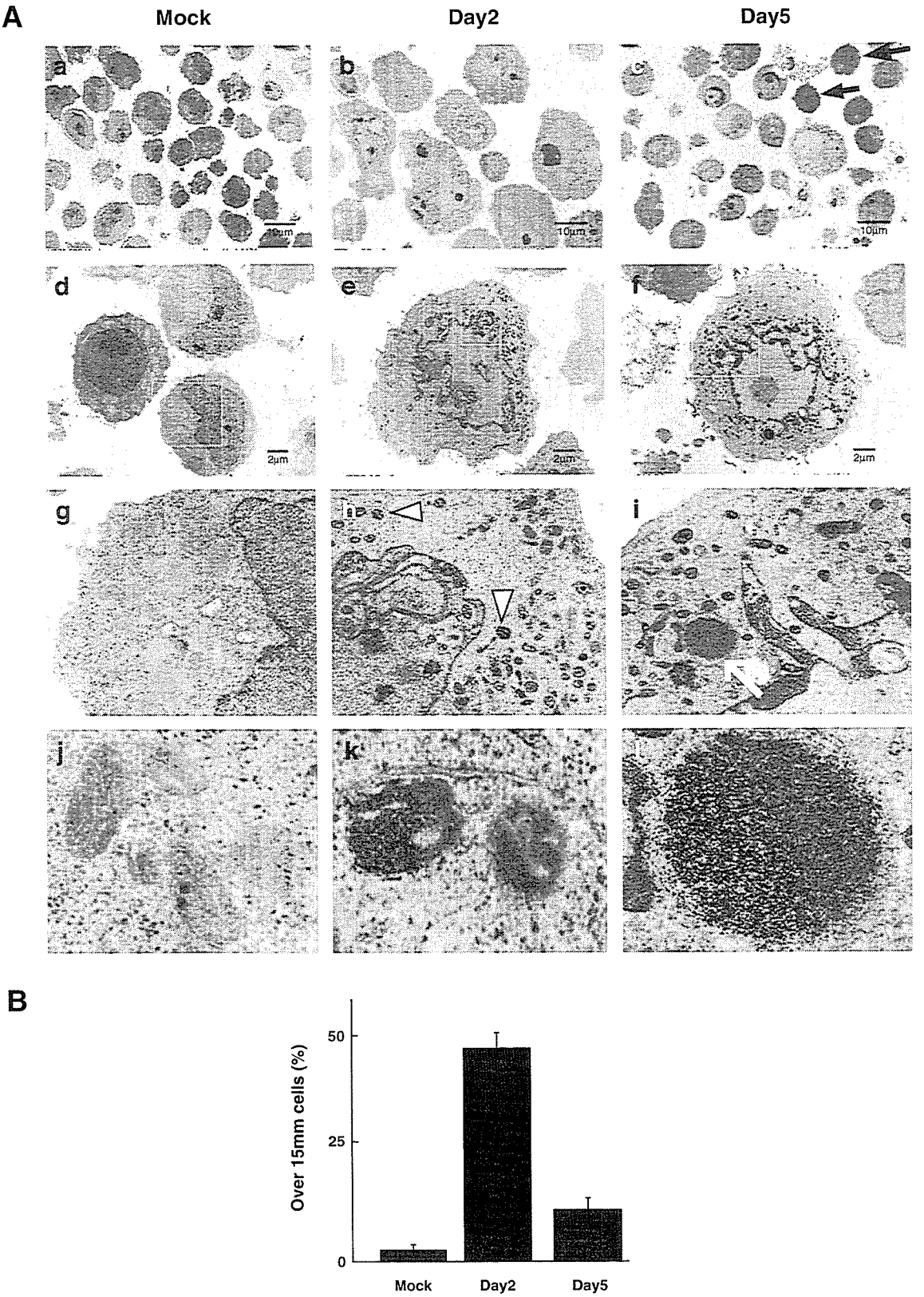

Fig. 2. Electron microscopy of B19 virus induced enlarged cells. UT7/Epo-S1 cells were infected with B19 virus, and fixed on days 2 (B), 5 (C). Mock-infected cells are used as control (A). Lower panels g–l respectively show the region outlined by white lines in above panels d–f. Black arrows indicate dying cells among the B19-infected cells (c). Open arrowheads indicate EM-dense mitochondria (h). White arrow (i) indicates EM-dense aggregates, possibly containing degraded mitochondria. Closed arrow heads (k) indicate the double-membrane structure. Mitochondria in mock infection (j), in B19 infection after day 2 (k) are also magnified. Scale bars, 10 μm (a–c), 2 μm (d–f) are indicated.